Intrinsic and synaptic determinants of receptive field plasticity in Purkinje cells of the mouse cerebellum

Ting-Feng Lin, Silas E. Busch, Christian Hansel*
Department of Neurobiology and Neuroscience Institute, University of Chicago, Chicago, Illinois, USA

Abstract

Non-synaptic ('intrinsic') plasticity of membrane excitability contributes to aspects of memory formation, but it remains unclear whether it merely facilitates synaptic long-term potentiation (LTP), or whether it plays a permissive role in determining the impact of synaptic weight increase. We use tactile stimulation and electrical activation of parallel fibers to probe intrinsic and synaptic contributions to receptive field (RF) plasticity in awake mice during two-photon calcium imaging of cerebellar Purkinje cells. Repetitive activation of both stimuli induced response potentiation that is impaired in mice with selective deficits in either intrinsic plasticity (SK2 KO) or LTP (CaMKII TT305/6VA). Intrinsic, but not synaptic, plasticity expands the local, dendritic RF representation. Simultaneous dendrite and axon initial segment recordings confirm that these dendritic events affect axonal output. Our findings support the hypothesis that intrinsic plasticity provides an amplification mechanism that exerts a permissive control over the impact of LTP on neuronal responsiveness.

Introduction

Synaptic plasticity shapes connectivity maps by selectively regulating synaptic weights, a mechanism long considered the core determinant of memory formation. However, membrane excitability, across neuron types and cellular compartments[1, 2, 3, 4, 5, 6], predicts spike output better than synaptic strength[7, 8], and may also play a role in memory representation[9]. Nevertheless, it remains unclear whether intrinsic plasticity, which tunes excitability, provides computational capacities beyond that achieved by synaptic plasticity alone, and whether this capacity is necessary or sufficient for memory formation.

Here, we study the isolated role of each plasticity mechanism in memory formation using cerebellar Purkinje cells (PCs) as a model and by leveraging transgenic mice with selective plasticity impairments. In order to optimize motor and non-motor learning[10], cerebellar PC dendrites maintain numerous synaptic connections carrying information that gets selectively integrated into a unitary axonal signal. Peripheral inputs traverse through mossy fibers to cerebellar granule cells, which provide an expansion recoding of sensory information through parallel fibers (PFs)[11, 12, 13]. Amid this wide array of sensory representations, only those PFs that drive postsynaptic activation form the PC receptive field (RF)[14, 15, 16, 17, 18, 19, 20, 21]. To adapt in a dynamic world, PC RFs need to continually update through neural plasticity[22, 23, 24, 25, 26], allowing the cerebellum to learn and process information based on experience[24, 25, 26, 27].

In brain slices, repetitive PF stimulation induces synaptic long-term potentiation (LTP) at PF-PC synapses[28, 29, 30, 31], thereby increasing PF-evoked PC firing[32]. Tetanus of PFs carrying somatosensory information in the intact circuit [17, 19, 21, 33] modifies the sensory-evoked simple-spike (SS) rate thus changing the PC somatosensory RF[27]. Furthermore, tetanization-induced SS potentiation has also been demonstrated with indirect PF activation by peripheral cutaneous stimulation[24, 25, 26]. PF tetanization co-induces intrinsic plasticity in PCs[2]. While EPSP amplitude alone is a poor predictor of spike output, intrinsic excitability is a better predictor[8]. Based on these *in vitro* observations, we therefore hypothesized that intrinsic plasticity acts as a permissive gate mechanism that regulates the propagation of distal EPSPs to the soma[7] and therefore determines how well LTP may control spike output. Here, we ask whether *in vivo* recordings from intact mice support this scenario.

To investigate the distinctive roles of these plasticity mechanisms, we conducted RF plasticity experiments in two transgenic mouse models with selective plasticity impairments: CaMKII-TT305/6VA[34], wherein a specific mutation blocking the inhibitory autophosphorylation of the postsynaptic protein CaMKII promotes synaptic long-term depression (LTD) at PF-PC synapses and prevents LTP induction[34], and SK2-KO[1, 2], wherein the absence of small conductance Ca^{2+} activated K^{+} (SK2) channels impairs intrinsic plasticity. Instead of recording SS frequency, we used two-photon microscopy to monitor calcium responses in PC dendrites as a readout of PF-mediated RFs. Consistent with earlier experiments documenting SS potentiation[24, 25, 26], we observed an increase in dendritic calcium responses to either airpuff stimulation of the paw or direct electrical stimulation of PFs following an induction protocol in awake wild-type mice. This potentiation was impaired in both CaMKII-TT305/6VA and SK2-KO mice, suggesting that synaptic plasticity alone –without the contributions of intrinsic plasticity– is insufficient for proper RF plasticity. Furthermore, PF tetanization resulted in distinct spatial patterns of calcium response on PC dendrites among different genotypes, highlighting the unique roles of synaptic versus intrinsic plasticity. By simultaneously monitoring PF-evoked responses across the dendrite, soma and axonal initial segment (AIS) of individual PCs, we identified correlated dendritic and AIS calcium responses, demonstrating that the dendritic events observed here do influence axonal calcium signals that likely accompany changes in spike output.

Results

Tactile stimulation elicits analog calcium signals in PC dendrites

While extensive research has explored phenomenological attributes of cerebellar tactile-RF plasticity through electrophysiological experiments[24, 25, 26, 27], the underlying mechanisms of cellular plasticity remain unclear. To obtain a highly reproducible readout of tactile-RFs in physiological conditions, we monitored single cell response properties during tactile stimulation using two-photon imaging of GCaMP6f-encoded calcium events in the cerebellum of awake mice (Fig. 1a).

To generate mice expressing GCaMP6f specifically in PCs, we co-injected AAV vectors encoding Cre-recombinase under the Purkinje cell protein 2 (Pcp2)/L7 promoter and Cre-dependent GCaMP6f (Fig. 1a) in Crus I, a region where somatosensory information is processed[14, 15, 17, 35, 36, 37, 38, 39]. To minimize motor-related signals obscuring sensory responsiveness, mice were trained to stay motionless on the experimental apparatus while airpuffs were delivered to a finger or wrist on the ipsilateral forelimb using a glass capillary tube (see Methods; Fig. 1b). During experiments, trials with motion were removed and a gentle airpuff stimulus (4-10psi) was used to avoid aversive responses and reduce activation of an olivary climbing fiber (CF) pathway which is sensitive to nociceptive input[18, 40, 41]. At the start of each experiment, we identified the region of lateral Crus I responsive to tactile stimulation of the paw and then focused our recording on the medial edge. Recording at the border of this tactile response area minimized the likelihood of failing to observe paw responsiveness while providing a high ceiling for potentiation of tactile responsiveness.

To characterize calcium responses to tactile stimulation of the forelimb, we compared spontaneous calcium events, randomly sampled from a 350ms time window before the airpuff stimulus, with time-locked responses during 0-350ms after stimulus onset. We tested responses to a range of stimulus strengths using a step increment of only 2psi (4, 6, 8, and 10psi) and observed an intensity-dependent increase in responsive trials (Fig. 1c), also reflected by the linear increase of response probability from 0.38 to 0.55 (Fig. 1d). By plotting the average calcium signal of all trials, we also observed a stimulus intensity-dependent increase in the size of calcium transients (Fig. 1e) though this could be attributable to a change in either the amplitude, probability, or both. Therefore, we separately plotted the average signals of responsive and non-responsive trials. We observed an increased amplitude of calcium transients when we excluded non-responsive trials (Fig. 1f), consistent with *in vitro* studies of PF responses in PCs[42, 43]. Quantitative analysis of the calcium transient further showed that both the probability (Fig. 1d) and the amplitude (Fig. 1g) depended on the stimulus strength. Based on the correlation coefficients of either probability or amplitude across stimulus conditions and normalized by the spontaneous events, we categorized PCs into stimulus intensity-dependent or -independent groups (Supplementary Fig. 1). Approximately 57% and 36% of PCs were categorized as the stimulus intensity-dependent group based on their probability and amplitude parameters, respectively. Initially, it was believed that *in vivo* dendritic calcium responses were exclusively due to CF input[44, 45], but subsequent studies showed that these responses could also occur without CF signal[46, 47, 48, 49]. In the current study, the dependence of evoked calcium transients on the small step change in stimulus intensity resembles the stereotypical PF response. Therefore, we conducted further examinations to determine whether calcium signals in awake mice exhibit tactile-RF plasticity, which is achieved through plasticity within the PF-PC pathway[25].

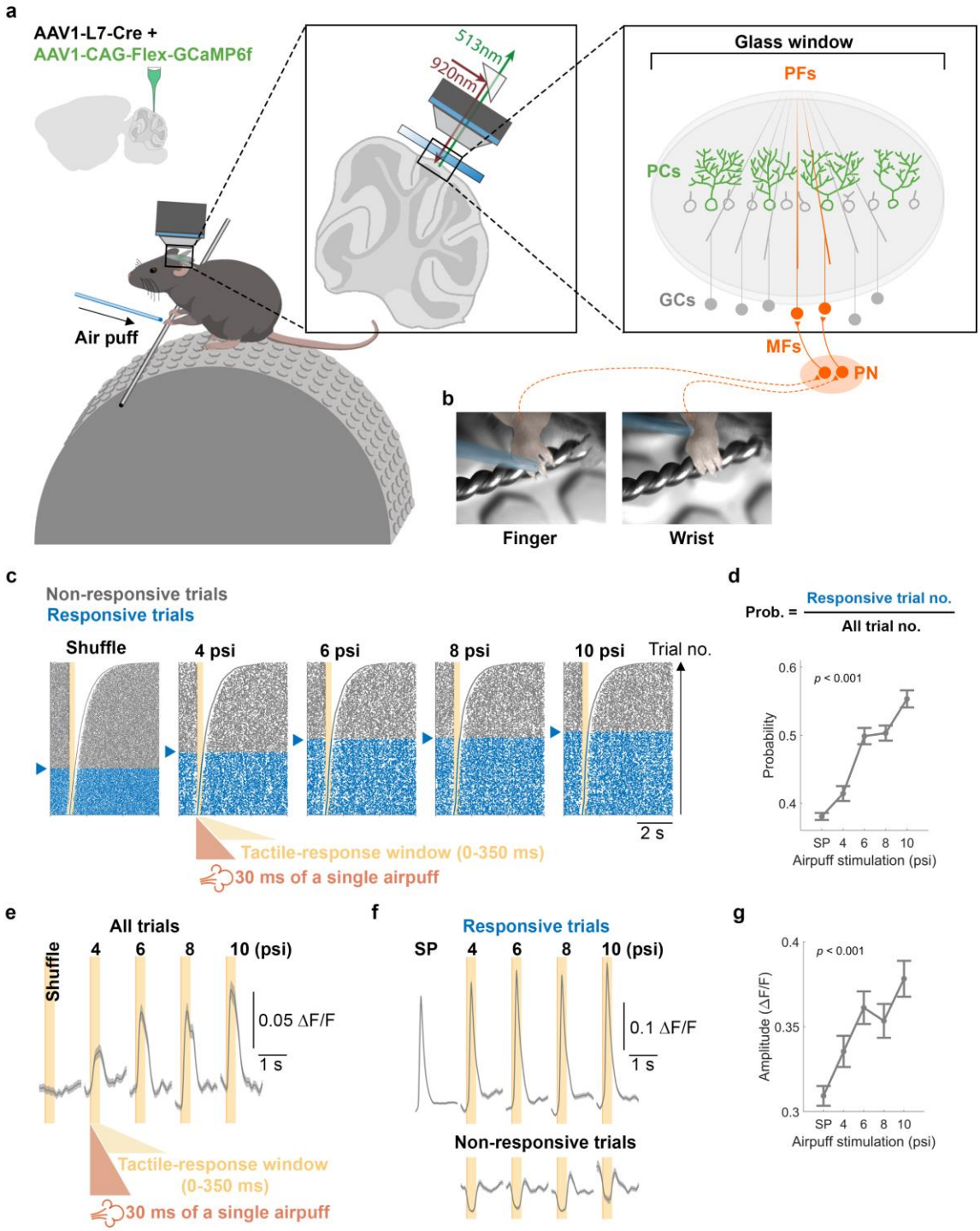

Figure 1 Stimulus-intensity dependence of PC responses to airpuff stimulation

a-b. AAV vectors were injected into Crus I of cerebellar cortex to express Cre-dependent GCaMP6f specifically in PCs. Cutaneous airpuff stimuli were applied to the finger or wrist of the forelimb while calcium responses in PC dendrites were recorded in ipsilateral Crus I under the two-photon microscope.

c. The raster plots depict both spontaneous and evoked responses to airpuff stimuli with varying pressures (4, 6, 8, and 10psi). The light orange area represents a 350ms shuffling window for

spontaneous events or a response window (0-350ms) for evoked events. Trials with detected events within the response window are categorized as responsive trials (indicated in blue), whereas those without are considered non-responsive trials (indicated in gray). Trials are sorted based on the timing of the first event following the initiation of either time window.

d. Probability (mean ± SEM) of detecting a calcium event within the defined time windows for spontaneous or responsive conditions. (One-way ANOVA: $F[4,1225] = 43.77$, $p < 0.001$)

e-f. Average calcium signals for all trials (**e**), responsive trials (top panel of **f**), and non-responsive trials (bottom panel of **f**).

g. Amplitudes (mean ± SEM) of calcium transients for spontaneous and responsive trials shown in **f**. (One-way ANOVA: $F[4,1223] = 8.21$, $p < 0.001$)

The post hoc pairwise comparisons using Tukey's HSD were shown in Supplementary Table 1-4. MFs, mossy fibers. PN, pontine nuclei. SP, spontaneous calcium events. (246 cells from 18 mice for all analyses)

Intrinsic and synaptic plasticity contribute to tactile-RF plasticity

To investigate plasticity of RFs to tactile stimulation ('tactile-RFs') in PCs, we recorded changes in calcium responses to tactile stimuli before and after application of a repetitive tactile induction protocol. To estimate the pre-tetanus baseline calcium response to an airpuff stimulus (8psi, 30ms), we performed 10-15 trials over 30min. Airpuff tetanization (8psi, 30ms) was then applied at 4Hz for 5min, reproducing a tactile-RF plasticity protocol described in previous studies[24, 25, 26]. We then recorded the conditioned calcium response for 1hr post-tetanization and divided the responses into 30min early and late post-tetanus periods (Fig. 2a). While intrinsic and synaptic potentiation have been suggested to underlie various forms of cerebellar learning[9, 50], their role in tactile-RF plasticity has not been tested before. To investigate this, we used two established loss-of-function models, SK2-KO[1] and CaMKII-TT305/6VA[34] mice, to assess the respective contributions of intrinsic and synaptic potentiation to tactile-RF plasticity. In SK2-KO mice, cellular specificity is achieved through L7 promotor-dependent Cre expression, selectively excising translation initiation sites for the *Kcnn2* (SK2) gene in PCs. CaMKII-TT305/6VA mice carry a global mutation; however, synaptic specificity is conferred by the unique function of CaMKII at PF-PC synapses. At these synapses, CaMKII promotes LTD[28, 31, 51, 52, 53, 54, 55], in contrast to LTP induction at most other types of glutamatergic synapses[50, 56].The TT305/6VA mutation blocks the inhibitory autophosphorylation of CaMKII, thus preventing the proper induction of LTP[34].

To assess tactile-RF plasticity, we defined a specific response time window of 0-200ms and asked whether tetanization would enhance the calcium response probability within this window, and whether it would alter the response amplitude (Fig. 2a). Both measures –response probability and amplitude– are relevant parameters to describe the RF of a neuron. The time window was selected to capture the early response that encodes peripheral inputs[21]. (Note that the overall calcium response may peak after 200ms, Fig. 2b; our analysis nevertheless focuses on early response amplitudes that better reflect immediate responses to sensory input.) The analysis of evoked calcium responses (Fig. 2b) showed that both calcium amplitude (Fig. 2c) and probability (Fig. 2d) were significantly potentiated after the induction protocol in wild-type mice, and that these changes were absent in SK2-KO and CaMKII-TT305/6VA mice as well as in wild-type mice under control conditions (see Methods). Here, the amplitude was measured as the maximum value within the time window because PF-evoked responses in a naturalistic condition are not expected to exhibit a sharp spike shape[48, 49] that can be reliably detected using defined criteria[46]. The original values of pre-tetanus baseline are provided in Supplementary Figure 2.

In conclusion, our airpuff tetanization experiments provide evidence for the potentiation of dendritic calcium responses under physiological conditions. Furthermore, our findings suggest that both intrinsic and synaptic mechanisms contribute to tactile-RF plasticity. To further investigate RF plasticity and elucidate the underlying mechanisms in PCs, we employed direct PF stimulation to better compare classic PF-LTP conditions as known from the slice literature to our studies *in vivo*. Moreover, direct PF stimulation also excludes the potential participation of graded CF responses[45, 48, 57], thereby enabling us to unequivocally address the synaptic input under investigation.

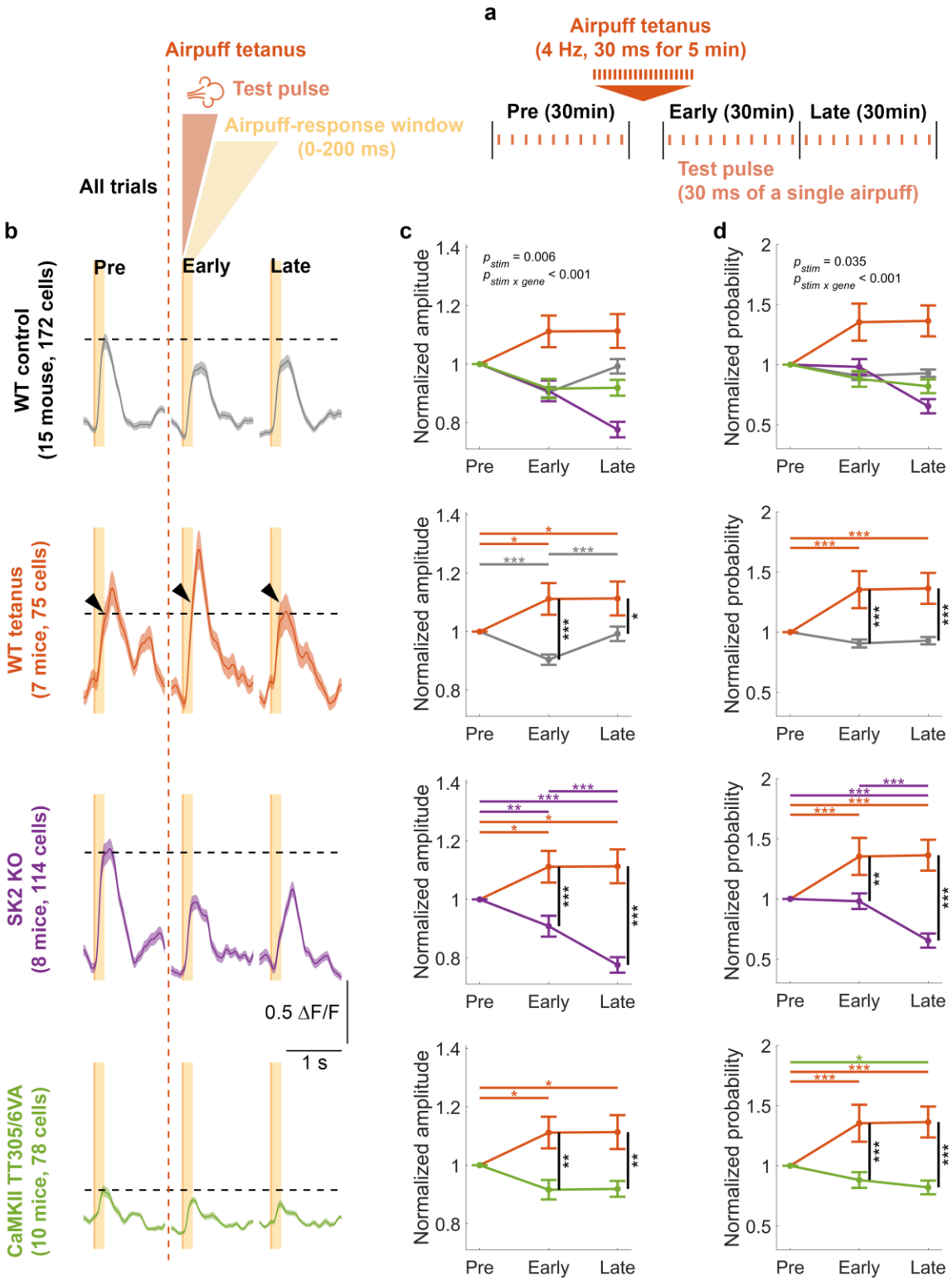

Figure 2 Tactile-RF plasticity on PC dendrites requires both synaptic and intrinsic plasticity

a. Schematic illustration of the experimental protocol. The recording began with a 30min baseline recording consisting of 10-15 trials, followed by an airpuff tetanus to potentiate the calcium response. The recording concluded with another 30min early and late post-tetanus recordings, each consisting of 10-15 trials.

b. Average calcium signals across trials from different genotypes. Arrowheads exemplify the calcium-event peaks within the 200ms time window.

c. Mean ± SEM of the normalized calcium-event amplitudes, calculated as the maximum value within the 0-200ms time window of individual trials. The data were normalized by the pre-tetanus amplitude. (Two-way repeated measure ANOVA: $F_{stim}[2,784] = 3.401$, $p = 0.034$; $F_{stim\ x\ gene}[6,748] = 11.404$, $p < 0.001$)

d. Mean ± SEM of the normalized probability of detecting a calcium event within the 0-200ms time windows. The data were normalized by the pre-tetanus probability. (Two-way repeated ANOVA: $F_{stim}[2,712] = 3.359$, $p = 0.035$; $F_{stim\ x\ gene}[6,712] = 8.956$, $p < 0.001$)

Asterisks denote the significance levels of post hoc comparisons using Tukey's HSD (*, $p < 0.05$; **, $p < 0.01$; ***, $p < 0.001$).

PF stimulation elicits local calcium responses

To establish compatibility with conventional *in vitro* experiments, we developed a platform that allows us to apply direct electrical stimulation to a bundle of PFs[58], which project >2mm in the medio-lateral axis orthogonal to the parasagittal alignment of PC dendrites[59, 60, 61], while simultaneously recording the corresponding calcium response in PCs of awake mice. Here, preparation stability was especially critical to ensure consistent stimulation of the same PF bundle throughout the experiment. Thus, the experimental setup closely resembled that of the tactile experiments wherein mice were trained to reduce motion while calcium signals were recorded from the same Crus I area. Though tactile stimulation of the paw was absent, mice were again trained to position their forelimbs on a horizontal bar to keep any cerebellar activation by posture consistent across experimental designs (Fig. 3a). During the experiment, a glass pipette filled with ACSF was inserted through a transparent silicone access port in the center of a 5mm glass cranial window to stimulate the PF bundle (Fig. 3b-3c). A stimulus train of 8 pulses applied at 100Hz successfully evoked calcium responses within a local region of each PC dendrite[49] reflecting the parasagittal width of the stimulated PF bundle (Fig. 3d). This stimulus protocol, resembling test pulse protocols *in vitro*[2, 34], was selected because stronger (more pulses or longer pulse duration) or weaker (fewer pulses) stimulations of PF bundles either oversaturated and damaged PFs or evoked diminutive PF inputs that fail to produce a detectable post-synaptic calcium signal.

Linescans of individual PC dendrites (Fig. 3e), and the corresponding local calcium activity reveal a spatiotemporal map that contrasts spontaneous from evoked signals (Fig. 3f-3g). Although spontaneous calcium signals exhibited a dynamic range of spatial distribution[48, 49, 62], most calcium events were relatively homogeneous across the entire dendrite. In contrast, evoked PF responses were restricted to a local area that intersected with the PF bundle (Fig. 3f). Quantified calcium signals before, during the peak, and at the end of the PF response (Fig. 3h) further demonstrate a time-locked local fluorescence peak with a clear drop-off at the edge of the stimulated PF-bundle input area. Our recording reproduced the previously reported stripe-like PF response in PCs[59, 60, 61], but at a subcellular scale, revealing sub-compartmental calcium response to PF stimuli, affirming previous observations *in vitro*[42, 43, 63, 64, 65, 66, 67].

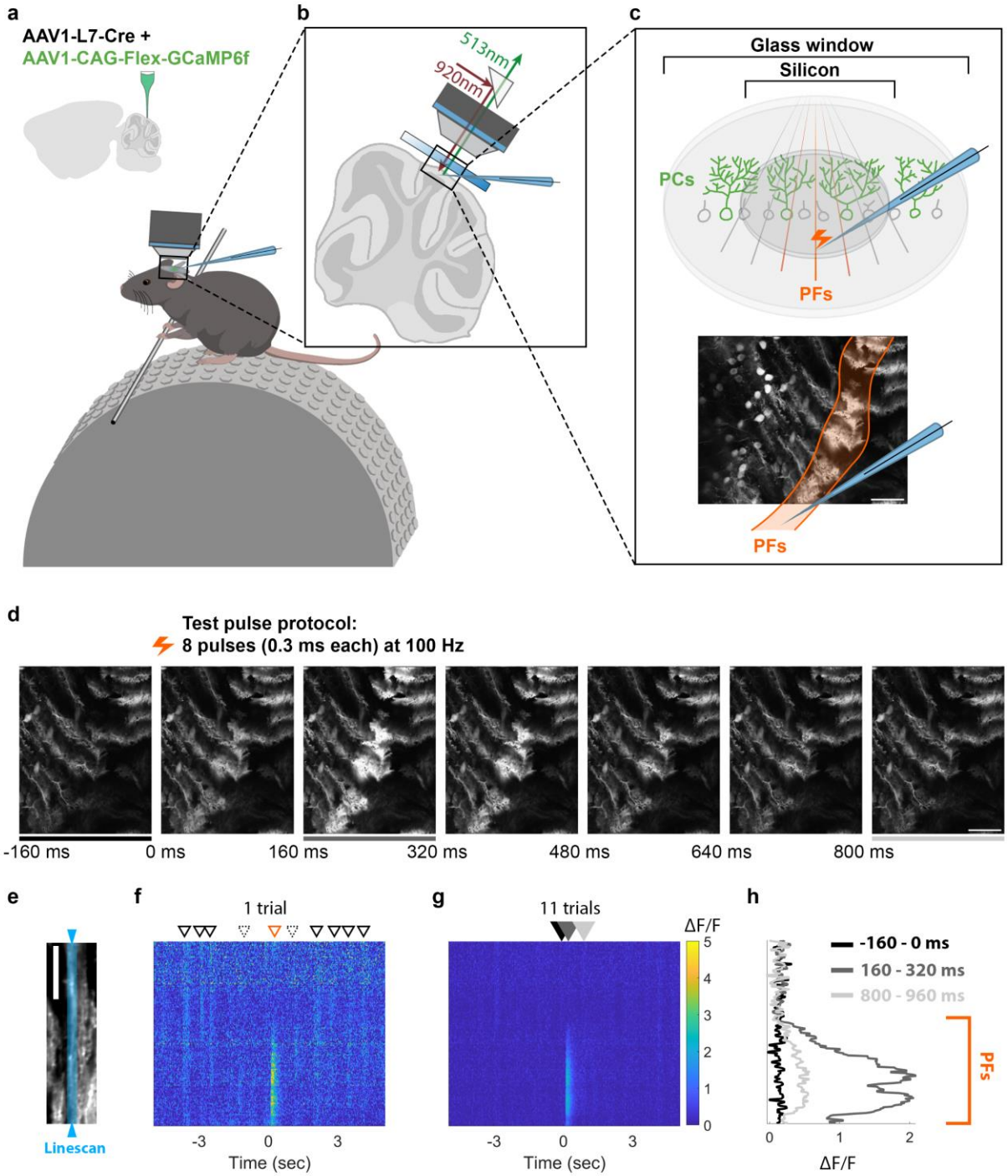

Figure 3 Localized calcium response in PC dendrites to PF stimulation

a. AAV vectors were injected into Crus I of cerebellar cortex to express Cre-dependent GCaMP6f specifically in PCs.

b-c. Schematic illustrations of the experimental setup of PF stimulation and calcium recording. Microelectrodes were used to apply electrical stimuli to a bundle of PFs in Crus I while recording calcium responses in PC dendrites under a two-photon microscope. The bottom panel of **c** shows a representative field of view during cerebellar recording and the resulting calcium response in PCs to the PF stimulus.

d. Two-photon images demonstrating calcium signals in PCs over time. Test pulses were applied at 0ms.

e-h. Linescan (blue shaded area) calcium signals of a single representative PC (**e**) are shown as spatiotemporal calcium maps from a single trial (**f**) and the average of 11 trials (**g**) during a 10sec recording period. (**f**) The triangles with solid black line denote global calcium responses, while the triangles with dashed line denote local calcium responses. The orange triangle indicates the PF stimulus. (**h**) The quantified fluorescence signals in different time windows, which are color-coded to correspond with lines and filled arrows shown in **d** and **g**, respectively. All scale bars are 50μm.

PF stimulation elicits analog calcium signals in PC dendrites

As with air puff stimuli, we tested calcium responses to increasing stimulus amplitudes in all genotypes. In these and the following plasticity experiments (Fig. 5), we selected a response time window of 50-400ms to capture calcium responses after half of the stimulus train was done (70ms in total) and leave sufficient time for response build-up. The average calcium signal showed a stimulus intensity-dependent increase in size across genotypes (Fig. 4a). When separating the average signals of responsive and non-responsive trials (Fig. 4b), we observed that both probability (Fig. 4c) and amplitude (Fig. 4d) are stimulus intensity-dependent. Correlation coefficients of normalized data across stimulus intensities, allowed the categorization of PCs into stimulus intensity-dependent or -independent groups (Supplementary Fig. 3). Regardless of genotype, over 85% of PCs were categorized as stimulus intensity-dependent, indicating that our transgenic models retain the standard anatomical structure of PF-PC innervation. Overall, the stimulus-intensity dependence of our observed calcium signals *in vivo* are highly consistent with that of the tactile experiments (Fig. 1) and previous studies both *in vitro*[42, 43] as well as *in vivo*[46, 48]. Crucially, the linear relationship between stimulus intensity and response amplitude is a stereotypical and conspicuous characteristic of PF-PC connections, identifying these calcium signals as likely PF-mediated. In the following experiments, we use these PF-mediated responses to characterize RF plasticity of PCs[17, 19, 21, 24, 25, 26, 27, 33].

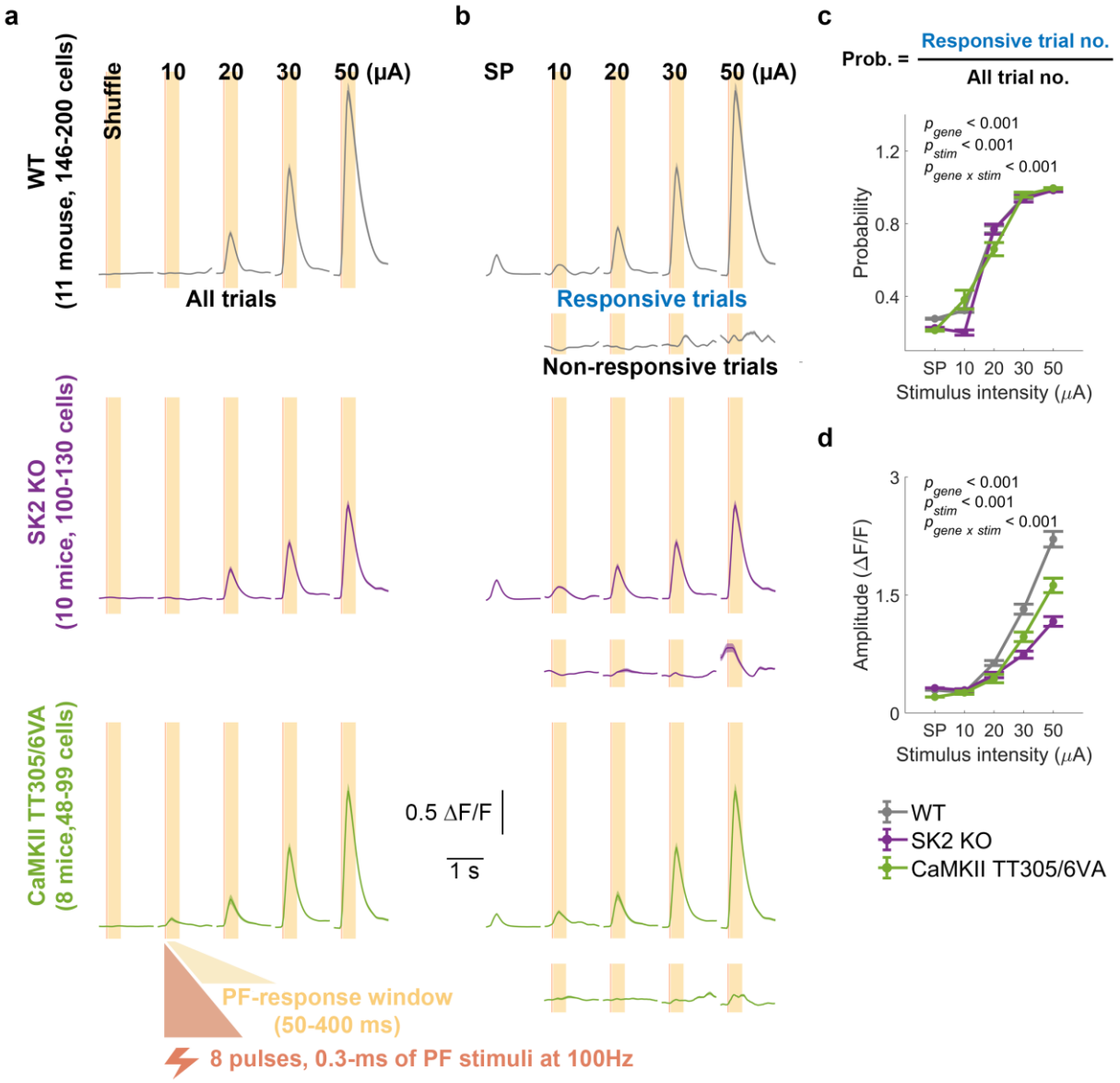

Figure 4 Dependence of PC response on PF stimulus intensity

a-b. Average calcium signals in response to PF stimuli with varying intensities (10, 20, 30, and 50μA) for all trials (**a**), responsive trials (top panel of **b**), and non-responsive trials (bottom panel of **b**), and. The light orange area represents a 350ms shuffling window for spontaneous events or a response window (50-400ms) for evoked events. Trials with detected events within the response window are categorized as responsive trials, whereas those without are considered non-responsive trials. SP, spontaneous calcium events.

c. Probability (mean ± SEM) of detecting a calcium event within the defined time windows for spontaneous or responsive conditions. (Two-way ANOVA: $F_{stim}[4,2939] = 2720.09$, $p < 0.001$; $F_{gene}[2,2939] = 13.82$, $p < 0.001$; $F_{stim\ x\ gene}[8,2939] = 11.51$, $p < 0.001$).

d. Amplitudes (mean ± SEM) of calcium transients for spontaneous and responsive trials shown in **b**. (Two-way ANOVA: $F_{stim}[4, 44701] = 3215.17$, $p < 0.001$; genotype, $F_{gene}[2,44701] = 484.06$, $p < 0.001$; $F_{stim\ x\ gene}[8, 44701] = 221.14$, $p < 0.001$).

The post hoc pairwise comparisons using Tukey's HSD were shown in Supplementary Table 5-12.

Intrinsic and synaptic plasticity contribute to PF-RF plasticity

To validate the potentiation of PC response to PF stimulation *in vivo*, and its dependence on synaptic and intrinsic plasticity, we employed direct electrical PF tetanization to induce potentiation of PC calcium responses. We selected the stimulus intensity that produced a reliable and intermediate response level (usually around 30μA) after testing the calcium response to a broad range of stimulus strengths (Fig. 4). The experimental procedure began with establishing a baseline by recording responses to a test stimulus (8 pulses, 0.3ms duration, 100Hz) for 10-12 trials over a 20min period. Next, to potentiate the calcium response, we applied PF tetanization (1Hz, 0.2ms pulses for 5min) and then recorded responses to test stimuli for 40min post-tetanus (Fig. 5a). The average calcium signals were separated into those immediately after the tetanus (early post-tetanus) or 20 minutes later (late post-tetanus) and are shown in Figure 5b. We observed an enhanced amplitude of calcium responses after PF tetanization in wild-type mice compared to no enhancement or a substantially lower effect in non-tetanized wild-type controls and both mutants (Fig. 5c-5d). Notably, although wild-type mice exhibited significantly higher potentiation than CaMKII-TT305/6VA mutants, the deficient LTP resulting from the mutation did not completely abolish the potentiation. Instead, CaMKII-TT305/6VA mutants still showed a modest but significant calcium potentiation, which is absent in SK2-KO mutants (bottom two panels of Fig. 5d), suggesting the existence of a contributor to this potentiation other than LTP. Non-responsive trials (Supplementary Fig. 4) were excluded from this analysis.

In these recordings, PF stimulation leads to well-timed responses that occur at high pre-tetanus probability (Supplementary Fig. 5), which remain unchanged after tetanization (Fig. 5e). Our *in vivo* observation of PF-RF potentiation aligns with previous studies of PF-induced potentiation conducted *in vitro*[28, 29, 30, 31, 32, 68], as well as in decerebrated[27] and anesthetized[25, 59, 60, 61] animals. Furthermore, we find that both synaptic and intrinsic potentiation play important roles in enhancing the postsynaptic calcium response as mutant mice lacking one or the other mechanism failed to exhibit the same degree of potentiation as wild-type mice.

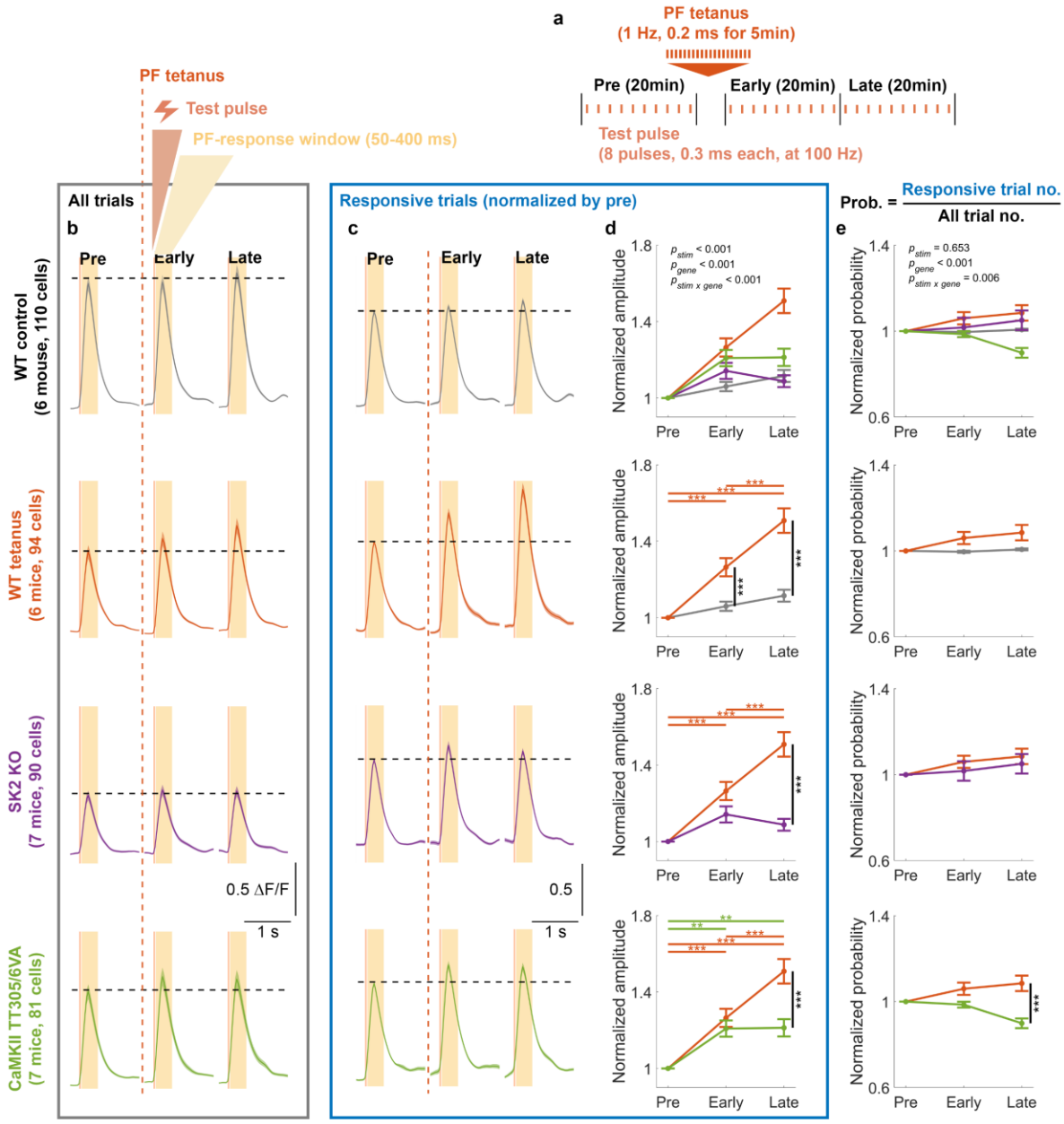

Figure 5 PF-RF plasticity on PC dendrites requires both synaptic and intrinsic plasticity

a. Schematic illustration of the experimental protocol. The recording began with a 20min baseline recording consisting of 10-12 trials, followed by a PF tetanus to potentiate the calcium response. The recording concluded with early and late post-tetanus recording periods, each consisting of 10-12 trials and lasting 20min.

b. Average calcium signals of different genotypes for all trials.

c. Normalized average calcium signals for responsive trials of each genotype. The signals are normalized by the average amplitude of pre-tetanus calcium transients. Only trials with detected events within the response window (50-400ms) were included.

d. Mean ± SEM of the normalized amplitudes of calcium transients for responsive trials shown in **c**. (Two-way ANOVA: $F_{stim}[2,1111] = 48.66$, $p < 0.001$; $F_{gene}[3,1111] = 21.69$, $p < 0.001$; $F_{stim\ x\ gene}[6,1111] = 8.95$, $p < 0.001$)

e. Mean ± SEM of the normalized probability of detecting a calcium event within the defined time windows. Data are normalized by the probability of pre-tetanus value. (Two-way ANOVA: $F_{stim}[2,1113] = 0.43$, $p < 0.653$; $F_{gene}[3,1113] = 6.95$, $p < 0.001$; $F_{stim\ x\ gene}[6,1113] = 3.02$, $p = 0.006$) Asterisks denote the significance levels of post hoc comparisons using Tukey's HSD (*, $p < 0.05$; **, $p < 0.01$; ***, $p < 0.001$).

Synaptic and intrinsic mechanisms show distinct spatial patterns of plasticity

Though *in vivo* dendritic signals of individual PC are often analyzed as a whole, local calcium dynamics in dendritic sub-compartments can play a critical role in PC function[48, 49, 62] and may reflect input structure and distinct plasticity types. Intrinsic plasticity is hypothesized to provide a widespread amplification function necessary to increase cellular gain and compliment the role of synaptic plasticity to locally tune the weight of individual inputs[9]. This hypothesis predicts that the unique mechanisms of each plasticity type would produce distinct spatial patterns of dendritic potentiation *in vivo*, reflecting the spatial differences between tuning synaptic weights versus cellular gain. To elucidate whether intrinsic and synaptic mechanisms of PF-RF plasticity operate with distinct spatial properties, we took advantage of the high spatial resolution afforded by our two-photon imaging approach to conduct a subcellular-level investigation.

While PCs from the two mutants displayed significantly lower potentiation compared to PCs in wild-type mice, the enhanced calcium response was not completely abolished, particularly in CaMKII-TT305/6VA mice. We propose that, unlike wild-type mice which exhibit intact plasticity function, SK2-KO PCs will show a particularly strong deficit in spatial spread of potentiation since they lack a global amplifier mechanism in dendrite-wide SK2 channel expression, while CaMKII-TT305/6VA PCs will maintain this plasticity component more strongly (Fig. 6a-6d).

To investigate the spatial pattern of PF-induced potentiation, we compared pre-tetanus baselines with values during early post-tetanus recordings, as this time period showed a more pronounced calcium enhancement than the late period in both mutants (Fig. 5). Linescan imaging along representative wild-type PC dendrites demonstrate that the potentiation of the calcium response consisted of a robust enhancement both within and around the responsive hotspot (dendritic pixels >0.9 Normalized ΔF/F, Fig. 6e and Supplementary Fig. 6a). We noticed that in a subpopulation of the SK2-KO PCs (16 out of 61 cells), not only did the modest potentiation occur exclusively within the hotspot, but the surrounding area was depressed (Fig. 6f and Supplementary Fig. 6b show representative PCs). In PCs from CaMKII-TT305/6VA mice, with intact intrinsic plasticity but impaired PF-LTP, potentiation of regions around hotspot was preserved, though the effect was less robust compared to wild types (Fig. 6g and Supplementary Fig. 6c).

To quantify the differences in spatial patterns across genotypes, we sorted linescan pixels by their fluorescence intensity to plot the cumulative length of those pixels as a function of fluorescence level (top panels of Fig. 6h-6j, derived from the individual PCs of Fig. 6e-6g). This provided the total dendritic length above a given fluorescence threshold (e.g., the hotspot threshold of 0.9, Fig. 6e-6h section 'B'), regardless of location along the dendrite. The cumulative length could then be compared between pre- and post-tetanus to obtain a tetanus-induced Δlength value. Genotype differences in Δlength revealed that the calcium signal expanded in wild-type and, to a lesser degree, CaMKII-TT305/6VA mice at all fluorescence levels (Fig. 6h and 6j). In contrast, while SK2-KO mice also exhibited a diminished potentiation, this effect was limited to the PF-responsive hotspot and the off-hotspot region (0.3-0.67 normalized ΔF/F) with intermediate fluorescence became more narrow (Fig. 6i).

Upon averaging the cumulative length and Δlength of all recorded PCs (Fig. 6k-6n), we observed a similar pattern to that exemplified by the representative individual data. However, as only a subset of SK2-KO PCs exhibited the hyper-localized 'narrowing' of the off-hotspot region, the effect was less pronounced in the broader cell population across animals (Fig. 6l). Nonetheless, the reduced expansion remained evident compared to the other two genotypes (Fig. 6n-6o). Across cells, the off-hotspot region was centered around 60μm cumulative length from the peak intensity of the hotspot (insets in Fig. 6k, 6l, and 6m), which represents the dendritic area ~30μm on either side of responsive peak in the PC cross section. As such, impairment of SK2-KO, but not CaMKII-TT305/6VA, plasticity in this region indicates the spatial influence of intrinsic mechanisms. Furthermore, the hotspot of both mutants showed less potentiation effect compared to wild types (Fig. 6p). As a result, the population Δlength distribution (Fig. 6n) revealed a leftward

shift in CaMKII-TT305/6VA PCs (reduced hotspot expansion) and a rightward shift in SK2-KO PCs (reduced off-hotspot expansion) compared to wild types. These differences were transient, as the difference in spatial patterns faded during the late post-tetanus period (Supplementary Fig. 7), primarily attributed to the transient potentiation of the off-hotspot area in CaMKII-TT305/6VA PCs (Supplementary Fig. 7l).

Taken together, these results demonstrate the spatial patterns of different plasticity mechanisms. Specifically, synaptic mechanisms alone (SK2 KO) sharpen the response area through local potentiation, while intrinsic mechanisms alone (CaMKII TT305/6VA) permit a widespread potentiation along the dendrite.

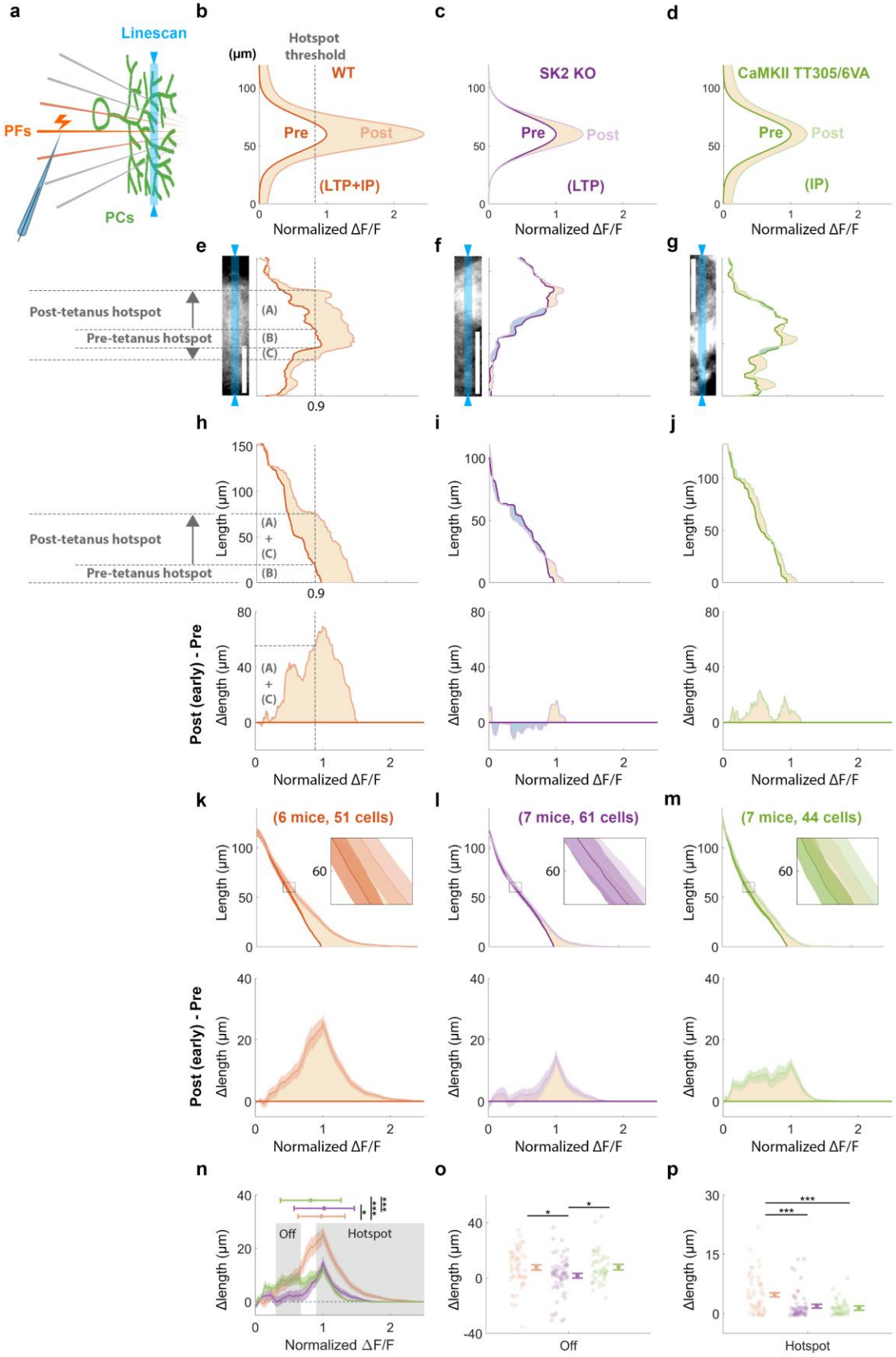
a
Linescan
PFs
PCs
b
Hotspot threshold
(µm)
WT
Pre
Post
(LTP+IP)
Normalized ΔF/F
c
SK2 KO
Pre
Post
(LTP)
Normalized ΔF/F
d
CaMKII TT305/6VA
Pre
Post
(IP)
Normalized ΔF/F
e
Post-tetanus hotspot
Pre-tetanus hotspot
(A)
(B)
(C)
0.9
f
g
h
Length (µm)
(A) + (C)
(B)
Post-tetanus hotspot
Pre-tetanus hotspot
0.9
i
j
Post (early) - Pre
Δlength (µm)
Normalized ΔF/F
k
(6 mice, 51 cells)
l
(7 mice, 61 cells)
m
(7 mice, 44 cells)
n
Off
Hotspot
Normalized ΔF/F
o
Off
p
Hotspot

377

Figure 6 Genotypic spatial patterns of PF calcium response during pre-tetanus and early post-tetanus periods.

a. Schematic diagram illustrates the linescan of PC dendrite calcium siganls (blue shaded area) in response to PF stimulation.

b-d. Conceptual models depict the hypothesized fluorescence signals along the PC dendrites of **a**, with dark and light traces showing pre- and (early) post-tetanus data, respectively. The X-axis represents the ΔF/F normalized by the maximum value of the pre-tetanus data.

e-g. Representative two-photon images of individual PCs from each genotype are shown in the left panels, with corresponding linescan fluorescence signals in the right panels. Blue shaded areas depict the linescan recording site. The dark and light traces represent pre- and post-tetanus data, respectively. The hotspot area (pixels with >0.9 normalized pre-tetanus ΔF/F) expanded from a length of (B) during the pre-tetanus period to a combined length of (A)+(B)+(C) during the post-tetanus period, thus the (A)+(C) represents Δlengths.

h-j. The top panel displays the cumulative lengths as a function of fluorescence level, while the bottom panel displays the corresponding Δlengths of the representative data shown in **e-g**. Cumulative lengths were obtained by summing up the dendritic length exhibiting the given fluorescence level, depicted as the dashed lines in **e** and the top panel of **h**. Δlengths were calculated by subtracting post-tetanus from pre-tetanus cumulative length, as indicated by the dashed lines in **h**.

k-m. For all cells from all mice in each group, mean ± SEM of cumulative lengths (top panel) and Δlengths (bottom panel) as in **h-j**.

n. Superimposed genotype Δlengths obtained from the bottom panel of **k-m**. The horizontal bar represents the median ± median absolute deviation of the distribution. Asterisks denote significance in distribution shift using Dunn & Sidák's approach (*, $p < 0.05$; **, $p < 0.01$; ***, $p < 0.001$) following Kruskal-Wallis test ($H[2] = 161.17$, $p<0.001$).

o-p. Mean ± SEM of Δlengths, calculated from the off-hotspot (**o**) and hotspot (**p**) as grey shaded areas shown in **n**, with individual cell values alongside. (One-way ANOVA: off-hotspot, $F[2,153] = 3.9$, $p =0.022$; hotspot, $F[2,153] = 12.45$, $p <0.001$) Asterisks denote the significance levels of post hoc comparisons using Tukey's HSD (*, $p < 0.05$; **, $p < 0.01$; ***, $p < 0.001$).

Dendritic calcium events relate to PC axonal output

Thus far, we have treated the measured dendritic calcium events as a read-out of PC activity without asking the question whether these events remain locally isolated or influence axonal spike output. Although the correlation between PF input and the SS output has been studied extensively in the past[32, 68], it remains undetermined whether dendritic calcium events – the measure used in our two-photon recordings from intact animals – reflect this input-output relationship as well. In previous studies, somatic and AIS calcium signals have been correlated with neural firing in PCs[69, 70]. To identify corresponding calcium activity across dendrites, soma, and AIS, we stimulated PF bundles and recorded PCs located in the sulcus of lobule Crus I (Fig. 7a), as opposed to the superficial gyrus, where PCs lie perpendicular to the imaging plane. This strategy allowed us to record all three cellular compartments simultaneously and draw ROIs separately based on their morphology (Fig. 7b). Figure 7c and 7d show the average signals of spontaneous and PF-evoked calcium transients, respectively, alongside the morphological structures shown in Fig. 7b. We observed that calcium activity in dendrites is often accompanied by calcium transients in the soma and AIS, regardless of whether it is generated spontaneously (Fig. 7c and Supplementary Fig. 8a-8c) or evoked by PF stimuli (Fig. 7d and Supplementary Fig. 8d-8f). To further examine their relationships, we conducted correlation analyses between calcium amplitude in dendrites and either the soma or AIS (Fig. 7e-7h). We observed a significant correlation between AIS and dendrites in response to PF electrical stimuli (Fig. 7h), indicating the impact of dendritic PF input on axonal activity. Additionally, we observed a suppression of calcium signal following the positive calcium transient (bottom panel of Fig. 7d), though the suppression level is not correlated with the amplitude of dendritic calcium transients ($R = -0.09$, $p = 0.908$, Pearson's correlation; Supplementary Fig. 8d and 8f). In conclusion, our data show that the PF-evoked dendritic calcium signals do indeed impact the somatic and axonal compartments in a manner that is likely to shape PC output.

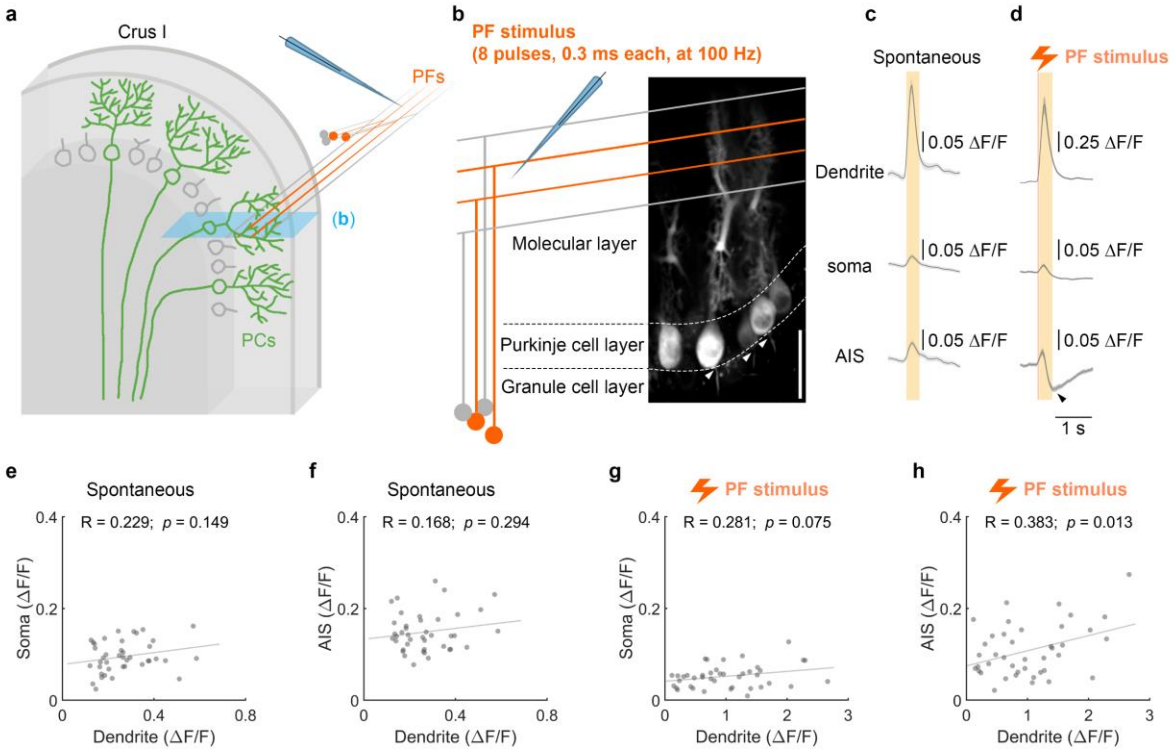

Figure 7 Correlation of activity between PC dendrites and AIS.

a. Schematic of microelectrode placement to apply electrical stimuli to a bundle of PFs while two-photon imaging was performed in the sulcus of lobule Crus I, where PCs lie horizontally. This allowed the dendrite, soma and AIS of each PC to be captured within single field of view. The blue shaded area represents the two-photon image plane, which yields a calcium image such as that shown in **b**.

b. Representative two-photon images of the dendrites, soma, and AIS of each PC captured by a single field of view. Arrows point to the AIS. The schematic diagram shows PF stimulation using a microelectrode to generate a calcium response.

c-d. Mean ± SEM of spontaneous calcium events (**c**) and evoked responses (**d**) of 41 cells from 5 mice. The black arrow in **d** indicates a suppression of AIS calcium signals following the initial response.

e-h. Maximum values of somatic and axonal calcium transients plotted against the maximum values of dendritic signals within the time window of 50-400ms after the initiation of the rising phase and stimulus for spontaneous events (**e-f**) and evoked events (**g-h**), respectively. Lines represent the linear regression fit, with R indicating the Pearson correlation coefficient and *p* indicating its significance.

Discussion

Our study demonstrates that both naturalistic tactile and direct PF tetanization can potentiate dendritic calcium responses in PCs of awake mice (Fig. 8). These effects are abolished in genetically modified mice with selective deficits in either synaptic (Fig. 8b) or intrinsic plasticity (Fig. 8c), demonstrating that both are necessary cellular determinants of the intact RF plasticity phenomenon. We also observed spatial aspects of this plasticity when describing differences in residual spatial plasticity patterns in SK2-KO and CaMKII-TT305/6VA PC dendrites, respectively. These observations assign a role in spreading the dendritic response to intrinsic plasticity. Finally, we identified a correlation between calcium activity in dendrites and AIS of PCs, demonstrating that the dendritic calcium events described here impact PC output and therefore provide a measure that relates to the spike output of these neurons.

These findings highlight the physiological significance of synaptic and intrinsic mechanisms in regulating PC dendritic computations and, consequently, in shaping its RFs in the awake animal. PCs play a central role in cerebellar function by selectively conveying information from diverse inputs as the sole output of the cerebellar cortex. Previous studies have reported that LTP and LTD can increase or decrease the SS frequency in response to PF or tactile stimuli, both *in vitro* and *in vivo*[24, 25, 26, 27, 32, 68]. However, the mechanisms that regulate input integration in the dendritic area remain unclear. To investigate this, we recorded calcium responses to tactile stimuli, which were previously thought to only reflect CF input *in vivo*[44, 45], but which have recently been shown to also occur without CF input[46, 47, 48, 49]. Previous studies might have missed weak and localized PF signals, possibly because PCs displaying CF responses have a lower likelihood of exhibiting PF responses, which is attributed to their inverse RFs[18]. We observed a potentiation in this tactile-evoked calcium response following an induction protocol, likely resulting from enhanced PF input, that can be diminished by mutations known to impact plasticity in PF-PC transmission. The calcium imaging data provides evidence for how plasticity mechanisms can enhance input at the dendritic level.

By analyzing the spatial patterns of calcium amplification, we observed distinct forms of potentiation (Fig. 6): local potentiation in the synaptic plasticity model (SK2 KO) and global potentiation in the intrinsic plasticity model (CaMKII-TT305/6VA). These novel observations provide insights into how different plasticity mechanisms modulate PF responses at different distances relative to the stimuli. Notably, only SK2 KO showed a limited expansion of the off-hotspot area (Fig. 6o), while both mutants displayed impaired amplitude potentiation of the hotspot compared to wild types (Fig. 6p). These observations suggest that only intrinsic plasticity exerts long-distance effects (~30µm relative to the center of PF stimuli in the image plane), while both mechanisms contribute to potentiation on the hotspot. Through their complementary roles, the interplay between synaptic and intrinsic plasticity enables the expansion of the RF without compromising input selectivity.

Local PF input does not always lead to faithful modulation of spike output. Instead, the summation of multiple inputs, whether temporal[8] or spatial[71], is required to exert an influence on spike output. Only then would the preceding PF inputs be considered physiologically significant. By up-regulating the excitability of compartmental or entire dendrites, the likelihood of inducing spiking activity can be enhanced[8]. In our investigation, we examined calcium signals in various regions of the PCs, including dendrites, soma, and AIS, simultaneously. Obtaining calcium signals from the soma and AIS has been challenging primarily due to the high firing frequency. However, through adjustments in the experimental configuration and by averaging signals from multiple trials, we were able to obtain clear calcium responses time-locked to the stimulus. The significant correlation between dendritic and axonal responses confirmed the impact of dendritic input on axonal output. Nevertheless, to gain a deeper understanding of the specific components contributing to calcium transients in the soma and axon, further electrophysiological recordings are necessary.

In our study, the absence of intrinsic plasticity in SK2-KO mice prevented almost all calcium potentiation, while CaMKII-TT305/6VA mice lacking synaptic potentiation exhibited a partially impaired yet significant residual potentiation effect (Fig. 5d and Fig. 6). These observations demonstrate that intrinsic plasticity does not merely enhance the effects of LTP, but instead exerts a permissive gating function (Fig. 8). Without intrinsic gate regulation, the amplitude of distal EPSPs remains poorly correlated with spike output[5,6], likely because intrinsic conductances across the dendrite attenuate the dendritic potential while it propagates towards the soma.

Our observations explain why delay eyeblink conditioning is impaired in SK2-KO mice where synaptic plasticity is intact (Titley et al., 2020[72]; see also Schreurs et al., 1998[73]). In dentate gyrus, suppressing synaptic plasticity impairs fear learning, but conditioned responses can be rescued by photoactivating engram cells[74]. This finding demonstrates that memory representation requires the conveyance of synaptic input to neuronal output (for a review, see Titley et al., 2017[9]). As we show here, this may be achieved through modulation of intrinsic excitability that selectively gates the influence of synaptic strength on somatic activation (Fig. 8a). Thus, as a general rule across neuron types, intrinsic plasticity may exert permissive control over the coupling of LTP to spike output, and thus the integration of neurons into engrams[9, 75]. This control would outlast transient roles assigned to intrinsic excitability, for example in the memory allocation hypothesis. There, allocation of neurons to a memory engram occurs when these neurons show high excitability at the time of learning, facilitating subsequent integration via LTP[76, 77]. It is conceivable that intrinsic plasticity has such facilitatory function in addition to a permissive gate function, without which, however, LTP remains without impact on spike output.

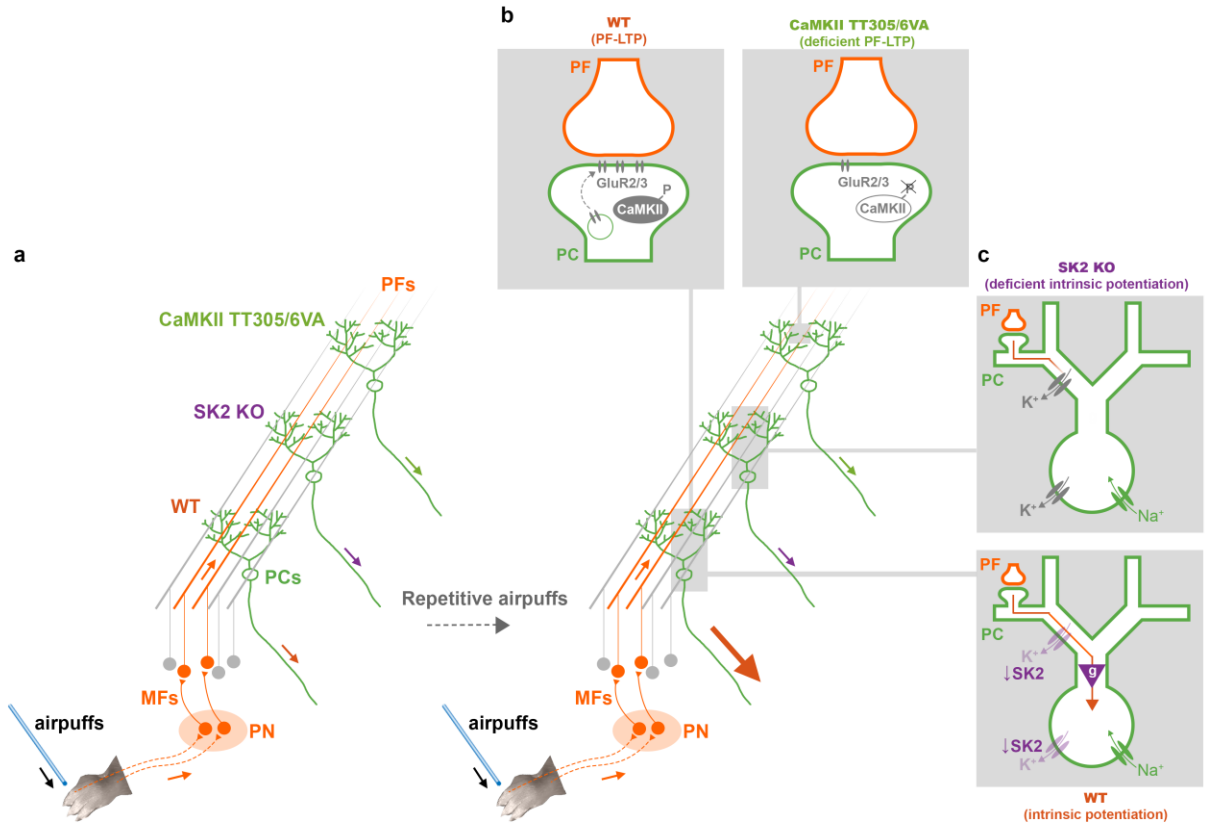

Fig. 8 RF potentiation requires both local PF-LTP and a SK2 gate control.
a. Potentiation of tactile response in PCs can be evoked by a repetitive PF stimulation. However, this potentiation is impaired without either PF-LTP (**b**) or intrinsic potentiation (**c**).
b. Blockade of CaMKII inhibitory autophosphorylation enhances the probability that CaMKII is in an active state, which at these synapses, in turn, lowers the probability for LTP.
c. SK2 regulation in dendrite and soma serve as a tunable gain operator (purple triangle) that gates the propagation of dendritic EPSPs towards the soma, and thus the effect of local PF-PC synaptic plasticity. PF-LTP without a coherent downregulation of SK2 channels is not sufficient to reveal the dynamic change in activity of PC dendrites, soma, or axon. Note that in SK2-KO mice, the baseline calcium responses are equally large or smaller than in WT mice (Supplementary Figs. 2 and Supplementary Figs. 5), pointing to a compensatory mechanism (potentially through upregulating different types of K+ channels as depicted with grey color in the top panel) that stabilizes excitability without enabling its plasticity. Thus, dendritic gating is not expected to be different under baseline conditions in SK2-KO mice.

Acknowledgements

We thank Drs. John F Disterhoft (Northwestern University) and Daniel Margoliash (University of Chicago) for comments on the manuscript, and members of the Hansel laboratory for insightful discussions. This study was supported by funding from the National Institute of Neurological Disorders and Stroke (NIH-NINDS Grant NS062771).

Data availability

The code is written in MATLAB R2021b and publicly available from GitHub: https://github.com/tingfenglin-ac/CerebellumRFplasticity

Code availability

Data presented in this study are saved as MAT-file (version 7.0) and publicly available from Mendeley Data: https://doi.org/10.5281/zenodo.8045156

References

1. Grasselli G*, et al.* SK2 channels in cerebellar Purkinje cells contribute to excitability modulation in motor-learning-specific memory traces. *PLoS Biol* **18**, e3000596 (2020).

2. Belmeguenai A*, et al.* Intrinsic plasticity complements long-term potentiation in parallel fiber input gain control in cerebellar Purkinje cells. *J Neurosci* **30**, 13630-13643 (2010).

3. Gill DF, Hansel C. Muscarinic Modulation of SK2-Type K(+) Channels Promotes Intrinsic Plasticity in L2/3 Pyramidal Neurons of the Mouse Primary Somatosensory Cortex. *eNeuro* **7**, (2020).

4. Ohtsuki G, Piochon C, Adelman JP, Hansel C. SK2 channel modulation contributes to compartment-specific dendritic plasticity in cerebellar Purkinje cells. *Neuron* **75**, 108-120 (2012).

5. Losonczy A, Makara JK, Magee JC. Compartmentalized dendritic plasticity and input feature storage in neurons. *Nature* **452**, 436-441 (2008).

6. Shim HG*, et al.* Long-Term Depression of Intrinsic Excitability Accompanied by Synaptic Depression in Cerebellar Purkinje Cells. *J Neurosci* **37**, 5659-5669 (2017).

7. Larkum ME, Zhu JJ, Sakmann B. Dendritic mechanisms underlying the coupling of the dendritic with the axonal action potential initiation zone of adult rat layer 5 pyramidal neurons. *J Physiol* **533**, 447-466 (2001).

8. Ohtsuki G, Hansel C. Synaptic Potential and Plasticity of an SK2 Channel Gate Regulate Spike Burst Activity in Cerebellar Purkinje Cells. *iScience* **1**, 49-54 (2018).

9. Titley HK, Brunel N, Hansel C. Toward a Neurocentric View of Learning. *Neuron* **95**, 19-32 (2017).

10. Popa LS, Ebner TJ. Cerebellum, Predictions and Errors. *Front Cell Neurosci* **12**, 524 (2018).

11. Nguyen TM*, et al.* Structured cerebellar connectivity supports resilient pattern separation. *Nature* **613**, 543-549 (2023).

12. Cayco-Gajic NA, Clopath C, Silver RA. Sparse synaptic connectivity is required for decorrelation and pattern separation in feedforward networks. *Nat Commun* **8**, 1116 (2017).

13. Litwin-Kumar A, Harris KD, Axel R, Sompolinsky H, Abbott LF. Optimal Degrees of Synaptic Connectivity. *Neuron* **93**, 1153-1164 e1157 (2017).

14. Eccles JC, Sabah NH, Schmidt RF, Taborikova H. Integration by Purkyne cells of mossy and climbing fiber inputs from cutaneous mechanoreceptors. *Exp Brain Res* **15**, 498-520 (1972).

15. Bower JM. Is the cerebellum sensory for motor's sake, or motor for sensory's sake: the view from the whiskers of a rat? *Prog Brain Res* **114**, 463-496 (1997).

16. Shambes GM, Beermann DH, Welker W. Multiple tactile areas in cerebellar cortex: another patchy cutaneous projection to granule cell columns in rats. *Brain Res* **157**, 123-128 (1978).

17. Thach WT, Jr. Somatosensory receptive fields of single units in cat cerebellar cortex. *J Neurophysiol* **30**, 675-696 (1967).

18. Ekerot CF, Jorntell H. Parallel fibre receptive fields of Purkinje cells and interneurons are climbing fibre-specific. *Eur J Neurosci* **13**, 1303-1310 (2001).

19. Bower JM, Woolston DC. Congruence of spatial organization of tactile projections to granule cell and Purkinje cell layers of cerebellar hemispheres of the albino rat: vertical organization of cerebellar cortex. *J Neurophysiol* **49**, 745-766 (1983).

20. Bosman LW*, et al.* Encoding of whisker input by cerebellar Purkinje cells. *J Physiol* **588**, 3757-3783 (2010).

21. Shimuta M, Sugihara I, Ishikawa T. Multiple signals evoked by unisensory stimulation converge onto cerebellar granule and Purkinje cells in mice. *Commun Biol* **3**, 381 (2020).

22. Roggeri L, Rivieccio B, Rossi P, D'Angelo E. Tactile stimulation evokes long-term synaptic plasticity in the granular layer of cerebellum. *J Neurosci* **28**, 6354-6359 (2008).

23. Jorntell H, Ekerot CF. Receptive field plasticity profoundly alters the cutaneous parallel fiber synaptic input to cerebellar interneurons in vivo. *J Neurosci* **23**, 9620-9631 (2003).

24. Marquez-Ruiz J, Cheron G. Sensory stimulation-dependent plasticity in the cerebellar cortex of alert mice. *PLoS One* **7**, e36184 (2012).

25. Ramakrishnan KB, Voges K, De Propris L, De Zeeuw CI, D'Angelo E. Tactile Stimulation Evokes Long-Lasting Potentiation of Purkinje Cell Discharge In Vivo. *Front Cell Neurosci* **10**, 36 (2016).

26. Jorntell H, Ekerot CF. Receptive Field Remodeling Induced by Skin Stimulation in Cerebellar Neurons in vivo. *Front Neural Circuits* **5**, 3 (2011).

27. Jorntell H, Ekerot CF. Reciprocal bidirectional plasticity of parallel fiber receptive fields in cerebellar Purkinje cells and their afferent interneurons. *Neuron* **34**, 797-806 (2002).

28. Hirano T. Depression and potentiation of the synaptic transmission between a granule cell and a Purkinje cell in rat cerebellar culture. *Neurosci Lett* **119**, 141-144 (1990).

29. Crepel F, Jaillard D. Pairing of pre- and postsynaptic activities in cerebellar Purkinje cells induces long-term changes in synaptic efficacy in vitro. *J Physiol* **432**, 123-141 (1991).

30. Shibuki K, Okada D. Cerebellar long-term potentiation under suppressed postsynaptic Ca2+ activity. *Neuroreport* **3**, 231-234 (1992).

31. Sakurai M. Synaptic modification of parallel fibre-Purkinje cell transmission in in vitro guinea-pig cerebellar slices. *J Physiol* **394**, 463-480 (1987).

32. Lev-Ram V, Mehta SB, Kleinfeld D, Tsien RY. Reversing cerebellar long-term depression. *Proc Natl Acad Sci U S A* **100**, 15989-15993 (2003).

33. Bengtsson F, Jorntell H. Sensory transmission in cerebellar granule cells relies on similarly coded mossy fiber inputs. *Proc Natl Acad Sci U S A* **106**, 2389-2394 (2009).

34. Piochon C, Titley HK, Simmons DH, Grasselli G, Elgersma Y, Hansel C. Calcium threshold shift enables frequency-independent control of plasticity by an instructive signal. *Proc Natl Acad Sci U S A* **113**, 13221-13226 (2016).

35. Romano V*, et al.* Potentiation of cerebellar Purkinje cells facilitates whisker reflex adaptation through increased simple spike activity. *Elife* **7**, (2018).

36. Ju C*, et al.* Neurons of the inferior olive respond to broad classes of sensory input while subject to homeostatic control. *J Physiol* **597**, 2483-2514 (2019).

37. Edge AL, Marple-Horvat DE, Apps R. Lateral cerebellum: functional localization within crus I and correspondence to cortical zones. *Eur J Neurosci* **18**, 1468-1485 (2003).

38. Cramer SW, Gao W, Chen G, Ebner TJ. Reevaluation of the beam and radial hypotheses of parallel fiber action in the cerebellar cortex. *J Neurosci* **33**, 11412-11424 (2013).

39. Ishikawa T, Shimuta M, Hausser M. Multimodal sensory integration in single cerebellar granule cells in vivo. *Elife* **4**, (2015).

40. Ekerot CF, Garwicz M, Schouenborg J. Topography and nociceptive receptive fields of climbing fibres projecting to the cerebellar anterior lobe in the cat. *J Physiol* **441**, 257-274 (1991).

41. Ekerot CF, Garwicz M, Schouenborg J. The postsynaptic dorsal column pathway mediates cutaneous nociceptive information to cerebellar climbing fibres in the cat. *J Physiol* **441**, 275-284 (1991).

42. Hartell NA. Strong activation of parallel fibers produces localized calcium transients and a form of LTD that spreads to distant synapses. *Neuron* **16**, 601-610 (1996).

43. Canepari M, Vogt KE. Dendritic spike saturation of endogenous calcium buffer and induction of postsynaptic cerebellar LTP. *PLoS One* **3**, e4011 (2008).

44. Kitamura K, Hausser M. Dendritic calcium signaling triggered by spontaneous and sensory-evoked climbing fiber input to cerebellar Purkinje cells in vivo. *J Neurosci* **31**, 10847-10858 (2011).

45. Gaffield MA, Bonnan A, Christie JM. Conversion of Graded Presynaptic Climbing Fiber Activity into Graded Postsynaptic Ca(2+) Signals by Purkinje Cell Dendrites. *Neuron* **102**, 762-769 e764 (2019).

46. Najafi F, Giovannucci A, Wang SS, Medina JF. Coding of stimulus strength via analog calcium signals in Purkinje cell dendrites of awake mice. *Elife* **3**, e03663 (2014).

47. Najafi F, Giovannucci A, Wang SS, Medina JF. Sensory-driven enhancement of calcium signals in individual Purkinje cell dendrites of awake mice. *Cell Rep* **6**, 792-798 (2014).

48. Roome CJ, Kuhn B. Dendritic coincidence detection in Purkinje neurons of awake mice. *Elife* **9**, (2020).

49. Roome CJ, Kuhn B. Simultaneous dendritic voltage and calcium imaging and somatic recording from Purkinje neurons in awake mice. *Nat Commun* **9**, 3388 (2018).

711 50. Jorntell H, Hansel C. Synaptic memories upside down: bidirectional plasticity at
712 cerebellar parallel fiber-Purkinje cell synapses. *Neuron* **52**, 227-238 (2006).
713
714 51. Sakurai M. Calcium is an intracellular mediator of the climbing fiber in induction of
715 cerebellar long-term depression. *Proc Natl Acad Sci U S A* **87**, 3383-3385 (1990).
716
717 52. Konnerth A, Dreessen J, Augustine GJ. Brief dendritic calcium signals initiate long-lasting
718 synaptic depression in cerebellar Purkinje cells. *Proc Natl Acad Sci U S A* **89**, 7051-7055
719 (1992).
720
721 53. Augustine GJ, Santamaria F, Tanaka K. Local calcium signaling in neurons. *Neuron* **40**,
722 331-346 (2003).
723
724 54. Coesmans M, Weber JT, De Zeeuw CI, Hansel C. Bidirectional parallel fiber plasticity in
725 the cerebellum under climbing fiber control. *Neuron* **44**, 691-700 (2004).
726
727 55. Titley HK, Kislin M, Simmons DH, Wang SS, Hansel C. Complex spike clusters and false-
728 positive rejection in a cerebellar supervised learning rule. *J Physiol* **597**, 4387-4406
729 (2019).
730
731 56. Elgersma Y*, et al.* Inhibitory autophosphorylation of CaMKII controls PSD association,
732 plasticity, and learning. *Neuron* **36**, 493-505 (2002).
733
734 57. Roh SE*, et al.* Direct translation of climbing fiber burst-mediated sensory coding into
735 post-synaptic Purkinje cell dendritic calcium. *Elife* **9**, (2020).
736
737 58. Roome CJ, Kuhn B. Chronic cranial window with access port for repeated cellular
738 manipulations, drug application, and electrophysiology. *Front Cell Neurosci* **8**, 379
739 (2014).
740
741 59. Reinert KC, Dunbar RL, Gao W, Chen G, Ebner TJ. Flavoprotein autofluorescence imaging
742 of neuronal activation in the cerebellar cortex in vivo. *J Neurophysiol* **92**, 199-211
743 (2004).
744
745 60. Gao W, Chen G, Reinert KC, Ebner TJ. Cerebellar cortical molecular layer inhibition is
746 organized in parasagittal zones. *J Neurosci* **26**, 8377-8387 (2006).
747
748 61. Wang X, Chen G, Gao W, Ebner T. Long-term potentiation of the responses to parallel
749 fiber stimulation in mouse cerebellar cortex in vivo. *Neuroscience* **162**, 713-722 (2009).
750
751 62. Busch SE, Hansel C. Climbing fiber multi-innervation of mouse Purkinje dendrites with
752 arborization common to human. *Science* **381**, (2023, In press).
753

754 63. Eilers J, Augustine GJ, Konnerth A. Subthreshold synaptic Ca2+ signalling in fine
755 dendrites and spines of cerebellar Purkinje neurons. *Nature* **373**, 155-158 (1995).
756
757 64. Finch EA, Augustine GJ. Local calcium signalling by inositol-1,4,5-trisphosphate in
758 Purkinje cell dendrites. *Nature* **396**, 753-756 (1998).
759
760 65. Eilers J, Takechi H, Finch EA, Augustine GJ, Konnerth A. Local dendritic Ca2+ signaling
761 induces cerebellar long-term depression. *Learn Mem* **4**, 159-168 (1997).
762
763 66. Hildebrand ME*, et al.* Functional coupling between mGluR1 and Cav3.1 T-type calcium
764 channels contributes to parallel fiber-induced fast calcium signaling within Purkinje cell
765 dendritic spines. *J Neurosci* **29**, 9668-9682 (2009).
766
767 67. Wang SS, Khiroug L, Augustine GJ. Quantification of spread of cerebellar long-term
768 depression with chemical two-photon uncaging of glutamate. *Proc Natl Acad Sci U S A*
769 **97**, 8635-8640 (2000).
770
771 68. Steuber V*, et al.* Cerebellar LTD and pattern recognition by Purkinje cells. *Neuron* **54**,
772 121-136 (2007).
773
774 69. Ramirez JE, Stell BM. Calcium Imaging Reveals Coordinated Simple Spike Pauses in
775 Populations of Cerebellar Purkinje Cells. *Cell Rep* **17**, 3125-3132 (2016).
776
777 70. Grundemann J, Clark BA. Calcium-Activated Potassium Channels at Nodes of Ranvier
778 Secure Axonal Spike Propagation. *Cell Rep* **12**, 1715-1722 (2015).
779
780 71. Ohtsuki G. Modification of Synaptic-Input Clustering by Intrinsic Excitability Plasticity on
781 Cerebellar Purkinje Cell Dendrites. *J Neurosci* **40**, 267-282 (2020).
782
783 72. Titley HK*, et al.* Intrinsic Excitability Increase in Cerebellar Purkinje Cells after Delay Eye-
784 Blink Conditioning in Mice. *J Neurosci* **40**, 2038-2046 (2020).
785
786 73. Schreurs BG, Gusev PA, Tomsic D, Alkon DL, Shi T. Intracellular correlates of acquisition
787 and long-term memory of classical conditioning in Purkinje cell dendrites in slices of
788 rabbit cerebellar lobule HVI. *J Neurosci* **18**, 5498-5507 (1998).
789
790 74. Ryan TJ, Roy DS, Pignatelli M, Arons A, Tonegawa S. Memory. Engram cells retain
791 memory under retrograde amnesia. *Science* **348**, 1007-1013 (2015).
792
793 75. Hansel C, Disterhoft JF. Why is synaptic plasticity not enough? *Neurobiol Learn Mem*
794 **176**, 107336 (2020).
795
796 76. Rogerson T*, et al.* Synaptic tagging during memory allocation. *Nat Rev Neurosci* **15**, 157-
797 169 (2014).

77. Yiu AP*, et al.* Neurons are recruited to a memory trace based on relative neuronal excitability immediately before training. *Neuron* **83**, 722-735 (2014).

78. El-Shamayleh Y, Kojima Y, Soetedjo R, Horwitz GD. Selective Optogenetic Control of Purkinje Cells in Monkey Cerebellum. *Neuron* **95**, 51-62 e54 (2017).

79. Chen TW*, et al.* Ultrasensitive fluorescent proteins for imaging neuronal activity. *Nature* **499**, 295-300 (2013).

80. Sheffield MEJ, Adoff MD, Dombeck DA. Increased Prevalence of Calcium Transients across the Dendritic Arbor during Place Field Formation. *Neuron* **96**, 490-504 e495 (2017).

81. Kostadinov D, Beau M, Blanco-Pozo M, Hausser M. Predictive and reactive reward signals conveyed by climbing fiber inputs to cerebellar Purkinje cells. *Nat Neurosci* **22**, 950-962 (2019).

Methods

Mice

All animal experiments were approved and conducted in accordance with the regulations and guidelines of the Institutional Animal Care and Use Committee of the University of Chicago (IACUC 72496). All mice were bred and maintained on a C57BL/6J background (The Jackson Laboratory, Bar Harbor, ME, USA). SK2 knockout mice (SK2-KO) were generated by crossing transgenic mice expressing CRE recombinase under the Purkinje cell (PC)-specific promoter Pcp2/L7 (JAX#010536) with transgenic mice with LOXP sites flanking the *Kcnn2* locus encoding SK2 protein (see the previous report[1] for detail). Mice with L7-Cre and homozygous SK2-LoxP were used for the experimental mutant group. CaMKII TT305/6VA genetically modified mice, which carry a global mutaiton[56], were obtained from Dr. Ype Elgersma (Erasmus Medical Center, The Netherlands). Wild-type mice used in the current studies were collected from the litter mates of both mutants confirmed by genotyping. All genotypes were regularly outcrossed with commercial wild-type C57BL/6J mice. P80-P120 adult mice were selected for the two-photon recording performed in this study, and the necessary surgeries were conducted 2-3 weeks prior to the recording. The tactile-receptive field (RF) plasticity experiments were conducted in 17 wild-type, 8 SK2-KO, and 10 CaMKII-TT305/6VA mice. The parallel fiber (PF)-RF plasticity experiments were conducted in 12 wild-type, 7 SK2-KO, and 7 CaMKII-TT305/6VA mice. Simultaneous recordings of dendrite, soma, and AIS were conducted in 5 wild-type mice. Animals of both sexes were used in all experiments. No sex differences were observed in the reported measures.

Cranial window and GCaMP injection surgeries

The surgeries for GCaMP injection and cranial window installation were performed 2-3 weeks prior to each experiment. The complete surgery was separated into two separate episodes: (1) headframe installation, and (2) virus injection along with cranial window installation. The mice were anaesthetized with ketamine/xylazine (100 and 10 mg/kg, respectively) and administered subcutaneous injections of meloxicam (1-2 mg/kg), buprenorphine (0,1 mg/kg), and sterile saline (1 ml). The surgeries were conducted under deep anesthesia, confirmed through a toe-pinch test. Body temperature was maintained at around 35-37°C using a DC Temperature Controller System (FHC, Bowdoin, ME, USA).

During the first surgery episode, the objective was to implant the headframe onto the skull. The fur on top and back of the skull was shaved, and the skin was sterilized using betadine and 70% ethanol. The skin around the occipital bone was excised, and underlying tissues were removed and cleaned. Muscle tendons connected to interparietal and occipital bones were cut to expose the back side of occipital bone. A custom-made titanium headframe (H. E. Parmer Company, Nashville, TN, USA) was installed via dental cement (Stoelting Co., Wood Dale, IL, USA).

After a recovery period of 2-3 days, the mice were prepared for the second surgery episode, following appropriate monitoring of infections and activity. A circular craniotomy with a diameter of 4mm was performed using a dental drill. The craniotomy was centered at 2.5mm laterally from the midline and 2.5mm caudally from lambda. The dura was carefully removed, exposing lobules simplex, Crus I, and anterior Crus II of the cerebellum. A glass pipette with a tip diameter of approximately 300µm was utilized to inject a total volume of 1800 nl of an AAV virus mix into two separate locations, 900 nl each, at a depth of 300µm below the pial surface of the medial and lateral Crus I (1.8mm and 3.2mm laterally from the midline, respectively). To express GCaMP6f in wild-type and CaMKII TT305/6VA mice, the AAV virus mix was prepared with 0.5% of full titer L7-Cre (AAV1.sL7.Cre.HA.WPRE.hGH.pA[78], Princeton Neuroscience Institute (PNI) Viral Core Facility, kindly provided by the lab of Dr. Samuel Wang at Princeton University), and 20% Cre-dependent GCaMP6f (AAV.CAG.Flex.GCaMP6f.WPRE.SV40[79]; Addgene, #100835). For SK2-KO mice, which exhibit constant expression of transgenic Cre recombinase under the control of

the L7 promotor, the AAV virus mix was prepared with 10% Cre-dependent GCaMP6f. Following each injection, the glass pipette carrying the AAV virus was held in the same position for 5min before withdrawal. Any potential debris and blood clots on the brain surface were carefully removed, and a two-layer glass window was installed using C&B Metabond dental cement (Patterson Dental Company, Saint Paul, MN, USA). The two-layer glass windows consisted of a 5mm glass window (Warner Instruments, Holliston, MA, USA, # CS-5R) and 4mm glass window (Tower Optical Corp, Boynton Beach, FL, # 4540-0495) adhered together using UV glue Norland Optical Adhesive 71 (Norland Products Inc., Jamesburg, NJ). In preparation for PF-stimulation experiments, a customized glass window with a central silicone access port was specifically created. To construct the access port, a 1.5mm hole was carefully drilled and subsequently filled with transparent Kik-Sil silicone adhesive (World Precision Instruments, Sarasota, FL, USA) at the center of the two-layer glass window[58].

Habituation

After virus injection, the experimenter visited the mice daily for 5-7 days to provide post-operative care. Once the mice exhibited exploratory behavior in their cage without showing signs of distress such as trembling or vocalization, the habituation training process began with handling of the mice. Typically, any signs of anxiety during handling diminished within two days, allowing the handling period to increase from 15min to 30min. The mice were handled in the vicinity of the recording area, so they could sniff and interact with the recording apparatus. Following two days of handling, the mice were introduced to a free-running treadmill. Their front paws were placed on a horizontal bar while heads were securely restrained via the head plate clamped on the left and right stands. During this process, the mice tended to use their hindlimbs to run while holding onto the frontal bar with their forelimbs. To alleviate anxiety, a partial wall supporting the side of the mouse body was used to enhance comfort. Throughout the training process, the duration of time spent on the treadmill increased gradually, ranging from 10 minutes to 2 hours per day, based on the mouse's comfort level. The objective of this study was to record calcium responses to tactile or PF stimulation while avoiding signals related to behavioral output, which may be encoded by the same region being imaged. To minimize motor signals, the mice were trained to remain still during stimulation. It was observed that training the mice on a locked treadmill significantly reduced their inclination to make movements. As soon as the mice exhibited relaxed behavioral patterns on the freely moving treadmill, the treadmill was periodically locked. A glass capillary tube for airpuff stimulation mounted on a three-axis manipulator was moved around the mice, so they could become accustomed to it. To habituate mice with airpuff stimulation without influencing the plasticity experiments, multiple airpuffs at 8 psi were delivered at irregular frequency to various areas of the right forelimb. The distance between the tube and the forelimb moved from far to close when the mice became habituated. Both the duration of treadmill locking and the frequency of airpuff delivery increased throughout the habituation process. In total, the mice underwent habituation for a period of 1-2 weeks until they showed no aversive responses to the airpuff (for tactile-RF experiments) and/or remained comfortably on the locked treadmill (for both tactile-RF and PF-RF experiments) for over two-hours.

Two-photon imaging

We conducted calcium imaging of the genetically encoded indicator GCaMP6f in ~~the~~ Crus I of the right hemisphere of head-fixed mice using a laser scanning two-photon microscope (Neurolabware, Los Angeles, CA, USA). For tactile-RF experiments, airpuff stimuli were delivered to the finger or wrist of the ipsilateral (right) forelimb. Any movement exhibited by the mice during the experiments led to a pause in the recording until the mouse returned to a steady state. Calcium images were obtained at a frame rate of 62 Hz with a pixel dimension 635x256 for tactile-RF experiments, and at a frame rate of 31 Hz with a pixel dimension of 635x512 for PF-RF experiments, using an 8KHz resonant scanning mirror. Excitation of GCaMP6f was achieved

using a 920-nm laser source provided by Mai Tai® DeepSee (Spectra-Physics, Milpitas, CA, USA), and the fluorescence emission was collected through a 16x water immersed objective (Nikon LWD 0.8NA, 3mm WD) using a GaAsP PMT (Hamamatsu Photonics, Shizuoka, Japan). The recording process was controlled by Scanbox software (Scanbox, Los Angeles, CA). To minimize background noise originating from ambient light, a custom-made light shield was fitted around the objective and the brain window.

To capture different aspects of PC structure in the imaging plane, the location and angle of the motorized objective lens were adjusted. For RF experiments, we obtained a cross-sectional view of PC dendrites from the top of crus I gyrus. In contrast, for the simultaneous recordings of dendrites, soma, and AIS, we acquired a side view of PCs in the Crus I sulcus (Fig. 7a-7b). During the RF experiments, the laser power was set to approximately 2% with a PMT gain of 0.95. This configuration allowed for prolonged recording while minimizing phototoxicity. For the simultaneous recording of the three PC structures, the laser power was increased to 10-15%, while the PMT gain was reduced to 0.6-0.7. This adjustment aimed to optimize the signal-to-noise ratio and enhance the detection of somatic and axonal signals, which display a relatively low fluctuation range of signals compared to the dendrite. With higher laser power, the use of a lower PMT gain helps prevent over-saturation in somatic and axonal fluorescence, ensuring accurate and reliable signal measurements.

Tactile stimulation

To deliver airpuffs to the paw or finger, we designed a horizontal grabbing bar positioned in front of the mice. By precisely adjusting the position of this bar relative to the mouse body, the mice exhibited a natural tendency to extend their forelimbs and comfortably position their front paws on the bar without retracting them in response to the airpuff stimulus. Before conducting any experiments, we assessed and identified the strongly responsive area in Crus I to tactile stimulation. Through a cranial window centered 2.5mm laterally from the midline, we consistently observed a robust calcium response to tactile stimuli in lateral Crus I. Once we defined this tactile response area, we focused our recording on the medial edge, where the calcium response was at an intermediate level. This approach increased the likelihood of observing a calcium response while avoiding saturation of response potentiation. For all tactile stimulation, we used a Picospritzer III (Parker Hannifin, Mayfield Heights, OH, USA) to deliver a single 30ms airpuff triggered at 10th sec of each 20sec trial, based on TTL signals sent from a PG4000A digital stimulator (Cygnus Technology, Delaware Water Gap, PA, USA). The airpuff was delivered through a 0.86mm diameter capillary tube placed approximately 2mm away from the finger or wrist. The PG4000A digital stimulator and two-photon imaging were synchronized via TTL signaling under control of scanbox software. Stimulus dependency was assessed over a duration of 40-60min, during which we collected data from 10-15 trials in each condition (4, 6, 8 and 10psi). In the plasticity experiments, we consistently used 8psi for both test and tetanus pulses. The plasticity experiment consisted of three periods: pre-tetanus, early post-tetanus and late post-tetanus, each lasting 30min and consisting of 10-15trials. The frequency of trials was intentionally kept low, approximately every 1-2min, to minimize the chance for evoking a potentiation effect during trial periods. Between the pre-tetanus and post-tetanus periods, airpuff tetanization at 8psi with a 30ms duration at 4Hz for 5min was delivered to elicit tactile-RF plasticity. By employing these gentle stimuli, we aimed to minimize the likelihood of evoking CF signals to the greatest extent possible[18, 40, 41]. As control experiments for wild-type mice, either the same airpuff tetanization was directed at an empty location equidistant to the head of the mouse (10 mice, 111 cells), or no airpuff tetanization at all (5 mice, 61 cells) for over 5min. No difference was observed between these two groups and were thus pooled together for the analysis shown in the Figure 2 and Supplementary Figure 2.

PF stimulation

During PF-RF experiments, we intended to remain the same experimental setup as the tactile-RF experiments to maximize their comparability. Calcium signals in Crus I were acquired when the mice were positioned on a locked treadmill and their forelimbs were placed on the horizontal grabbing bar. However, instead of using the airpuff stimulation described earlier, electrical stimulation was applied to a bundle of PFs. A glass pipette filled with ACSF was inserted through the silicone access port at the center of the glass brain window. Often, a thin layer of transparent scar tissue developed after removal of the dura between the glass window and the surface of the cerebellum. Successfully positioning the glass pipette usually required a slight overshoot of insertion to pierce the scar tissue, followed by retracting the pipette tip back to the surface area of the molecular layer. The position and angle of the glass pipette was controlled by a PatchStar motorized micromanipulator (Scientifica, Uckfield, UK), while the calcium response was assessed and identified in epifluorescence mode. To evoke calcium response to PF stimulation, an electrical pulse was generated using a constant current source SIU91A (Cygnus Technology), triggered by an EPC-10 amplifier (HEKA Elektronik, Lambrecht/Pfalz, Germany) under the control of Patchmaster software (HEKA Elektronik). The Patchmaster software operated on a different computer than the Scanbox software, and they were synchronized through TTL signaling between the EPC-10 amplifier and the Scanbox board. A successful PF bundle stimulation could generate a calcium response in PC dendrites cross a medio-lateral distance of more than 2mm, and this was underestimated due to the folding structure of cerebellar cortex and the size of the craniotomy. To record the PF response and avoid artifact from a direct stimulation of PCs, the glass pipettes were placed at least 100μm away, in the medio-lateral axis, from the PCs being recorded. Once the glass pipette was in place and a reliable calcium response could be detected by epifluorescence, stimulus-dependence assessment and PF-RF plasticity experiments were conducted using two-photon microscopy.

During each 10sec trials, at the 5sec mark, an electrical stimulus of 8 pulses with 0.3ms duration at 100Hz was delivered. Stimulus dependence was assessed over a duration of 40min, during which we collected data from 10-12 trials in each condition (10, 20, 30 and 50μA). A stimulus intensity evoking an intermediate level of calcium response, around 30μA, was used for the plasticity experiments. The plasticity experiment consisted of three periods: pre-tetanus, early post-tetanus and late post-tetanus, each lasting 20min (as opposed to 30min for airpuff stimulation) and consisting of 10-12 trials. The frequency of trials was intentionally kept low, approximately every 1-2min, to minimize the chance for evoking a potentiation effect. Between the pre-tetanus and post-tetanus periods, PF tetanization was introduced by delivering a single pulse with a duration of 0.3ms at 1Hz for 5min using the same stimulus intensity as the test pulse to elicit PF-RF plasticity.

Image analysis

The time-series frames obtained from the experiments were converted into TIFF files. To ensure consistency among trials after motion correction, all trials were concatenated along the z-axis, representing the time series, into a single file. Subsequently, the concatenated time-series images underwent motion correction using a custom-made MATLAB script (MathWorks, Natick, MA, USA) based on whole frame cross-correlation[80] (kindly provided by the lab of Mark Sheffield, University of Chicago). Cellular regions of interests (ROIs) were manually selected in ImageJ based on volumetric cell reconstruction conducted after each experiment. For PF-RF plasticity experiments, the ROIs encompassed the entire PC dendrite, regardless of whether only a portion of the dendrite intersected with stimulated PF bundle, as indicated by a hotspot within a PC dendrite. This approach allowed us to capture the potentiation that transformed silent synapses into active synapses. The calcium intensity of each ROI was measured, and ΔF/F values were calculated using the following equation: $(F_t-F_0)/F_0$, where F_t represented the raw calcium intensity of the time series, and F_0 was set as the 20th percentile of each fluorescence trace[81], serving as the baseline fluorescence. The resulting ΔF/F values were then subjected to low-pass filtering using a five-

frame moving window smoothing function. For spike detection, a custom interactive MATLAB GUI was utilized, offering automatic detection with a manual correction function. The spike detection thresholds, including the threshold and prominence threshold, were set at 0.09, which is approximately equivalent to one standard deviation of the pre-stimulus baseline.

In the analysis of the spatial pattern of calcium distribution during PF-RF plasticity experiments, PC populations that displayed calcium response across the entire dendritic cross-section were excluded. This selection methods allow us to differentiate between hotspot and off-hotspot area within each PC. A line was manually drawn along the cross-section of the PC dendrite, and linescan data was obtained using the reslice function in ImageJ. The *output spacing* parameter was set to approximately 15μm, corresponding to the thickness of PC cross-section. The pixel-by-pixel ΔF/F along the scanned line was calculated using the same approach as described earlier for the cellular ROIs.

Statistical analysis

All data analyses and visualizations were conducted using MATLAB R2021b. To represent calcium signals, the calcium traces from different trials of individual PC were averaged, and then the average ± SEM across PCs was calculated. To show calcium traces without stimulus (Fig. 1e and Fig. 4a), calcium signals were obtained from set duration time windows (350ms), randomly sampled within -4.5 to -0.5sec relative to the stimulus onset. Representative spontaneous spikes (Fig. 1f and Fig. 4b) were selected from -4.5 to -0.5sec relative to the stimulus onset, and their peaks were temporally aligned. The calcium-event probability of each PC was calculated as the number of trials that exhibited a detected spike peak within the defined time window, divided by the total number of trials. Throughout the article, calcium-event amplitude generally refers to the amplitude of detected spikes, except in the context of tactile-RF plasticity (Fig. 2c and Supplementary Fig. 2), as well as the simultaneous recordings of dendrite, soma and AIS (Fig. 7 and Supplementary Fig. 8, for detailed discussion see later paragraph), where the amplitude specifically refers to the maximum value within the designated time window (0-200ms and 50-400ms, respectively). This approach was used in tactile-RF plasticity experiments, taking into account that the slow rising and the low amplitude characteristics of the naturalistic PF-mediated calcium event[48, 49] cannot be reliably detected using a defined criteria[46]. Given the variability in spike timing, the calcium event amplitude of each PC was calculated by averaging the amplitudes of individual calcium responses (Fig. 1g, 2c, 4d, 5d), rather than using the peak of the trial-averaged trace (Fig. 1e, 2b, 4b, 5c).

To evaluate the differences in calcium-event probability or amplitude attributed to the different factors (stimulus intensity, stimulus tetanization and genotypes), we performed statistical analysis using one-way ANOVA, two-way ANOVA, or two-way repeated measure ANOVA. Post hoc pairwise comparisons were then conducted using Tukey's HSD test. Stimulus intensity-dependent and stimulus intensity-independent PCs were classified based on the Pearson correlation coefficient, with a stimulus intensity-dependent threshold set at $R > 0.5$ and $p < 0.5$, calculated using the 5 data points (spontaneous events and 4 stimulus intensities) within each PC.

To quantify the differences in spatial patterns, we calculated the cumulative length by sorting and summing up pixels of dendritic linescans based on their fluorescence level normalized by the maximum value of pre-tetanus response, disregarding the original dendritic location (Fig. 6e and 6h). Through this method, we can estimate the length of PF-responsive area (hotspot). The difference in cumulative length —Δlength— was calculated by subtracting the pre-tetanus value from the post-tetanus value (Fig. 6h). Δlength represents the spatial expansion of hotspot or off-hotspot. To assess the difference in the distribution of Δlength (Fig. 6n and Supplementary Fig. 7m), a non-parametric Kruskal-Wallis test was conducted, followed by post hoc pairwise comparison using Dunn & Sidák's approach.

To analyze the simultaneous recording of dendrite, soma, and AIS, we averaged data from different trials without employing our spike detection method. This was necessary because the

somatic and AIS signals were relatively noisy compared to dendritic signals and exhibited distinct time constants which could not be compared using the same event deconvolution parameters. The average trace revealed the presence of positive transients, and the maximum values within a time window of 50-400ms were measured for each individual cell compartment. These maximum values were then used for further correlation analysis, as shown in Figure 7e-7h. The correlation coefficient was performed using the Pearson correlation coefficient.

Supplementary Figure

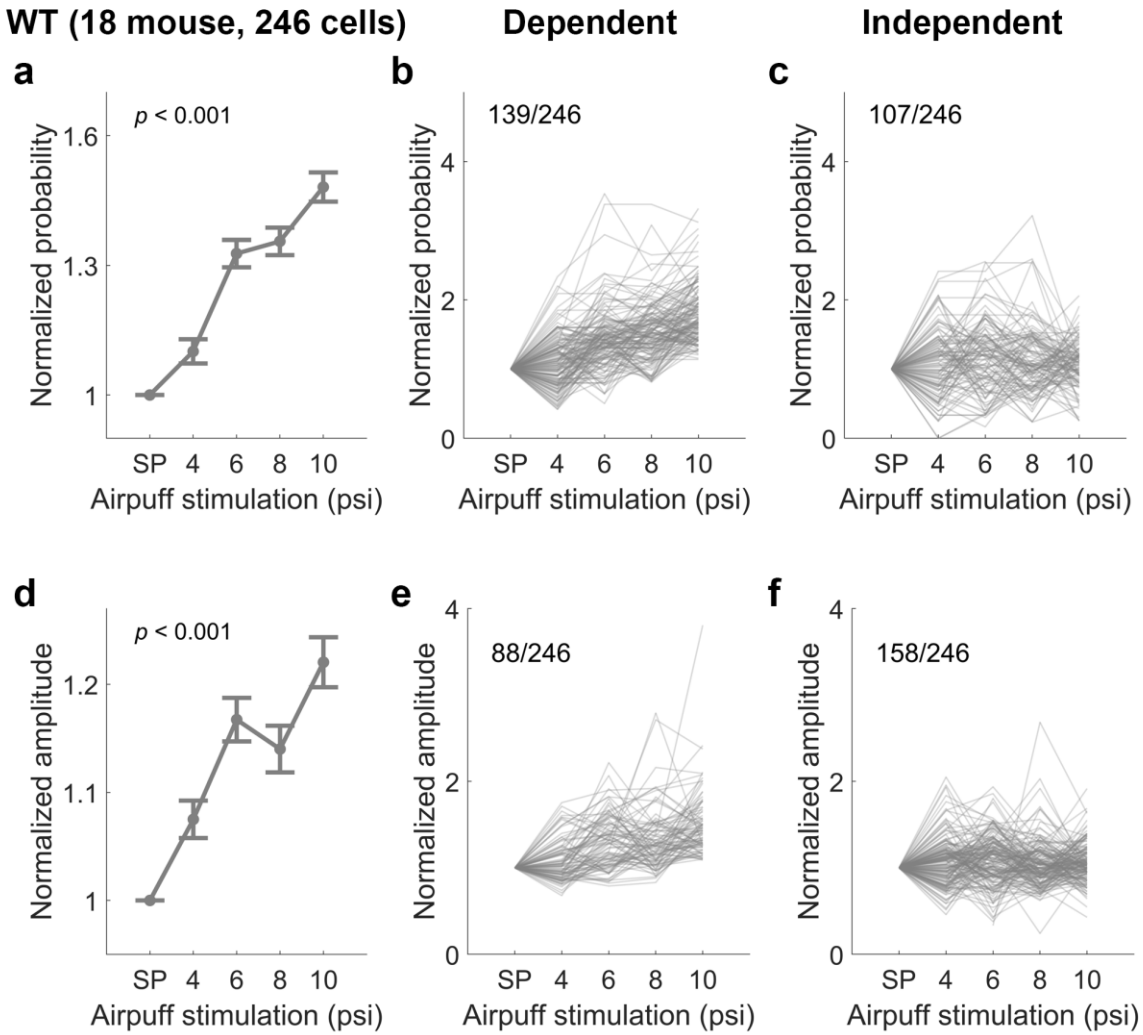

Supplementary Fig. 1 Stimulus intensity-dependent and -independent PC responses to airpuff stimulation

a. Calcium-event probability as depicted in Fig. 1d normalized by the spontaneous values of individual cells. (mean ± SEM). (One-way ANOVA: $F[4,1225] = 48.64$, $p < 0.001$)

b-c. Stimulus intensity-dependent (**b**) and stimulus intensity-independent cells (**c**) categorized according to the correlation coefficient of normalized probability. The labels on top of the plots indicate the number of designated cells out of the total number.

d. Calcium-event amplitude as depicted in Fig. 1g normalized by the spontaneous values of individual cells. (mean ± SEM). (One-way ANOVA: $F[4,1223] = 21.25$, $p < 0.001$)

e-f. Stimulus intensity-dependent (**e**) and stimulus intensity-independent cells (**f**) categorized according to the correlation coefficient of normalized probability. The labels on top of the plots indicate the number of designated cells out of the total number.

The post hoc pairwise comparisons of **a** and **d** using Tukey's HSD were shown in Supplementary Table 3-4. SP, spontaneous calcium events.

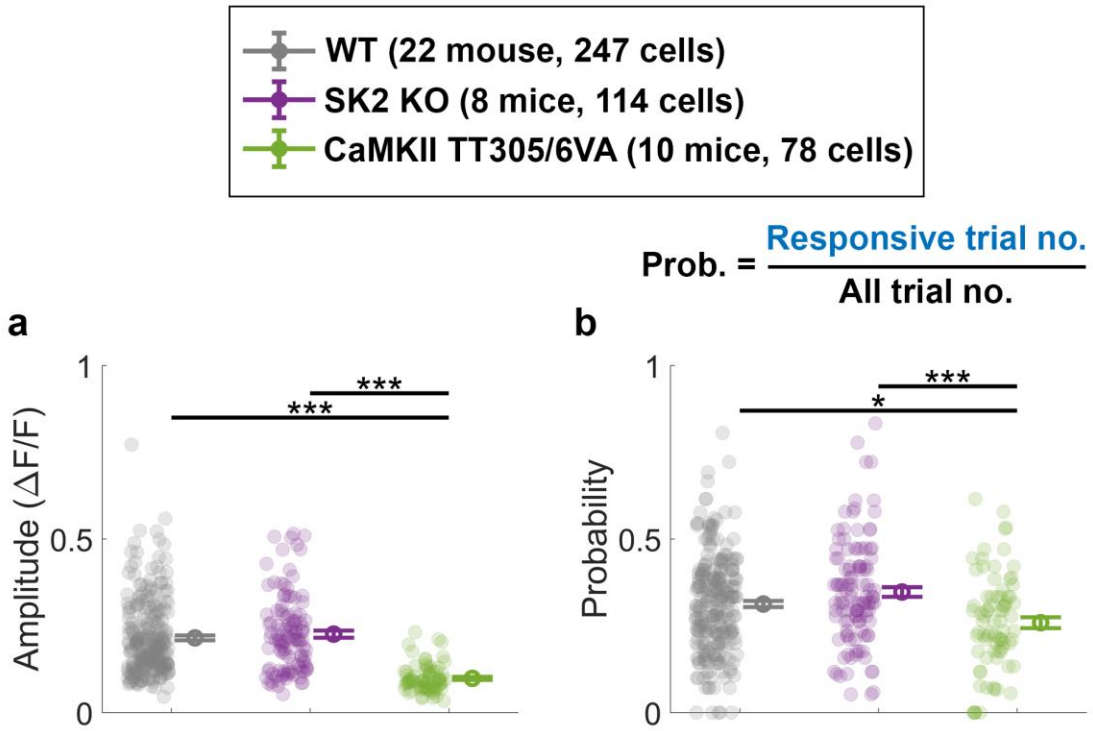

Supplementary Fig. 2 Amplitude and probability of pre-tetanus calcium events in response to airpuff stimulation

a. Mean ± SEM and individual cell values of the pre-tetanus amplitudes of calcium transients, calculated as the maximum value within the 0-200ms time window of individual trials. (One-way ANOVA: $F[2,436] = 46.91$, $p < 0.001$)

b. Mean ± SEM and individual cell values of the pre-tetanus probability of detecting a calcium event within the defined time window of 0-200ms. (One-way ANOVA: $F[2,436] = 8.92$, $p < 0.001$) Asterisks denote the significance levels of post hoc comparisons using Tukey's HSD (*, $p < 0.05$; **, $p < 0.01$; ***, $p < 0.001$).

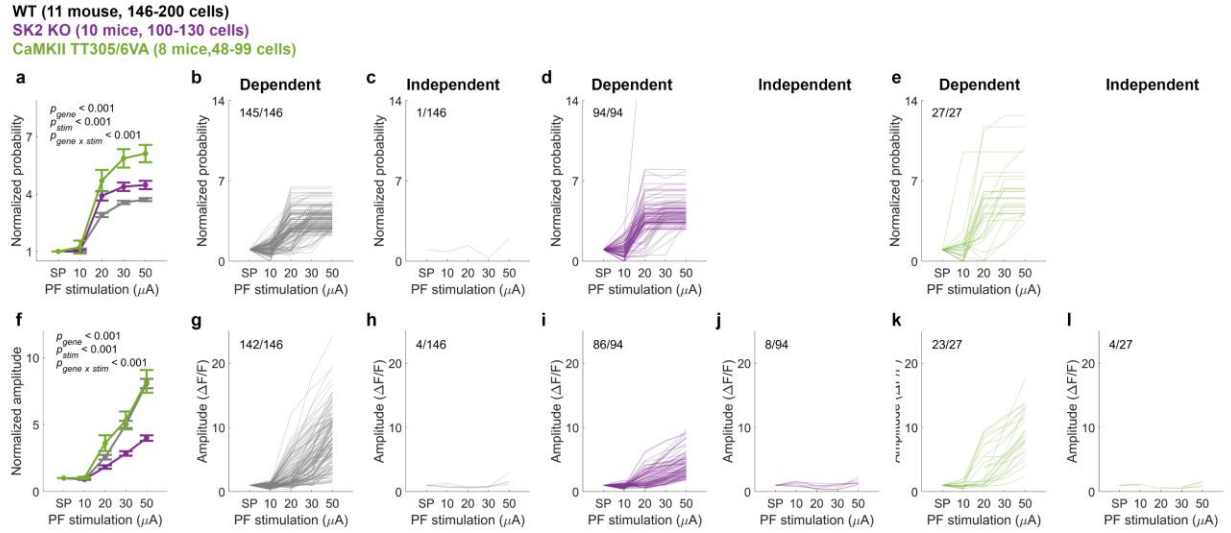

Supplementary Fig. 3 Stimulus intensity-dependent and stimulus intensity-independent PC responses to PF stimulation

a. Calcium-event probability (mean ± SEM) as depicted in Fig. 4c normalized by the spontaneous values of individual cells. (Two-way ANOVA: $F_{stim}[4,1320] = 283.89$, $p < 0.001$; $F_{gene}[2,1320] = 55.62$, $p < 0.001$; $F_{stim\ x\ gene}[8,1320] = 9.67$, $p < 0.001$).

b-e. Stimulus intensity-dependent (**b, d and e**) and stimulus intensity-independent cells (**c**) categorized according to the correlation coefficient of normalized probability. The labels on top of the plots indicate the number of designated cells out of the total number. The data are derived from the data presented in **a**, but only include the trials that were tested under all four different stimulus conditions.

f. Calcium-event amplitude (mean ± SEM) as depicted in Fig. 4d normalized by the spontaneous values of individual cells. (Two-way ANOVA: $F_{stim}[4,1296] = 185.13$, $p < 0.001$; $F_{gene}[2, 1296] = 60.56$, $p < 0.001$; $F_{stim\ x\ gene}[8, 1296] = 17.76$, $p < 0.001$).

g-l. Stimulus intensity-dependent (**g, l and k**) and stimulus intensity-independent cells (**h, j and l**) categorized according to the correlation coefficient of normalized probability. The labels on top of the plots indicate the number of designated cells out of the total number. The data are derived from the data presented in **f**, but only include the trials that were tested under all four different stimulus conditions.

Only cells that were tested with all four stimulus intensities were included in the categorization, which include wild type (146 cells), SK2 KO (94 cells), CaMKII TT305/6VA (27 cells). The post hoc pairwise comparisons of **a** and **f** using Tukey's HSD were shown in Supplementary Table 9-12. SP, spontaneous calcium events.

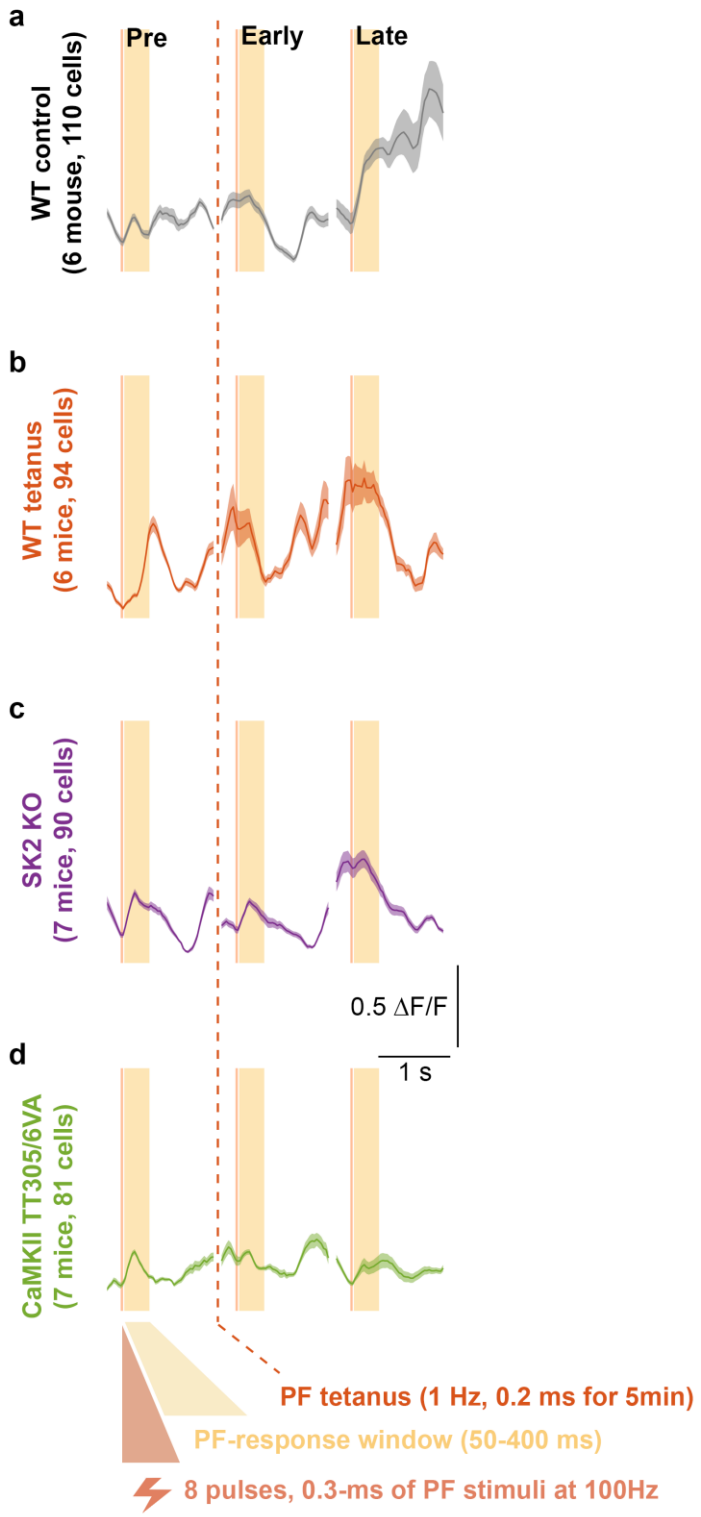

Supplementary Fig. 4 Average calcium signals for non-responsive trials within time window of 50-400ms in tactile-RF experiments

a-d. Average calcium signals for non-responsive trials, defined by time windows of 50-400ms.

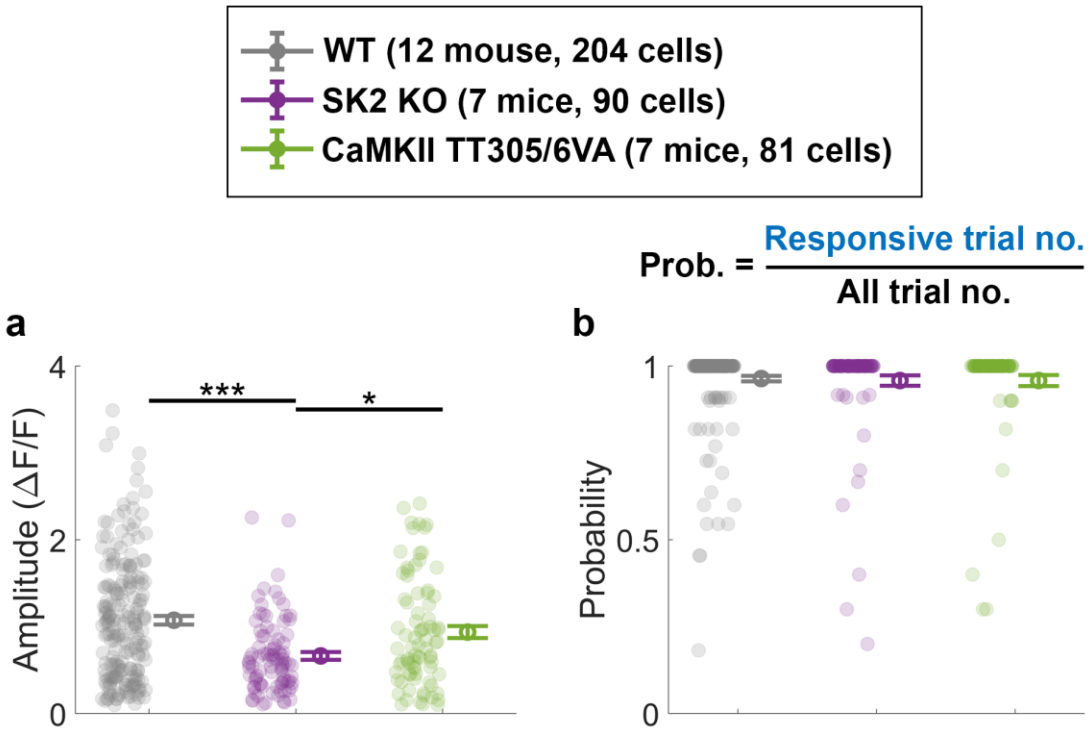

Supplementary Fig. 5 Amplitude and probability of pre-tetanus calcium events in response to PF stimulation.

a. Mean ± SEM of the pre-tetanus amplitudes of calcium transients for responsive trials shown in Fig. 5d. (One-way ANOVA: $F[2,374] = 13.35$, $p < 0.001$)

b. Mean ± SEM of the pre-tetanus probability of detecting a calcium event within the defined time window of 50-400ms. (One-way ANOVA: $F[2,374] = 0.09$, $p = 0.910$)

Asterisks denote the significance levels of post hoc comparisons using Tukey's HSD (*, $p < 0.05$; **, $p < 0.01$; ***, $p < 0.001$).

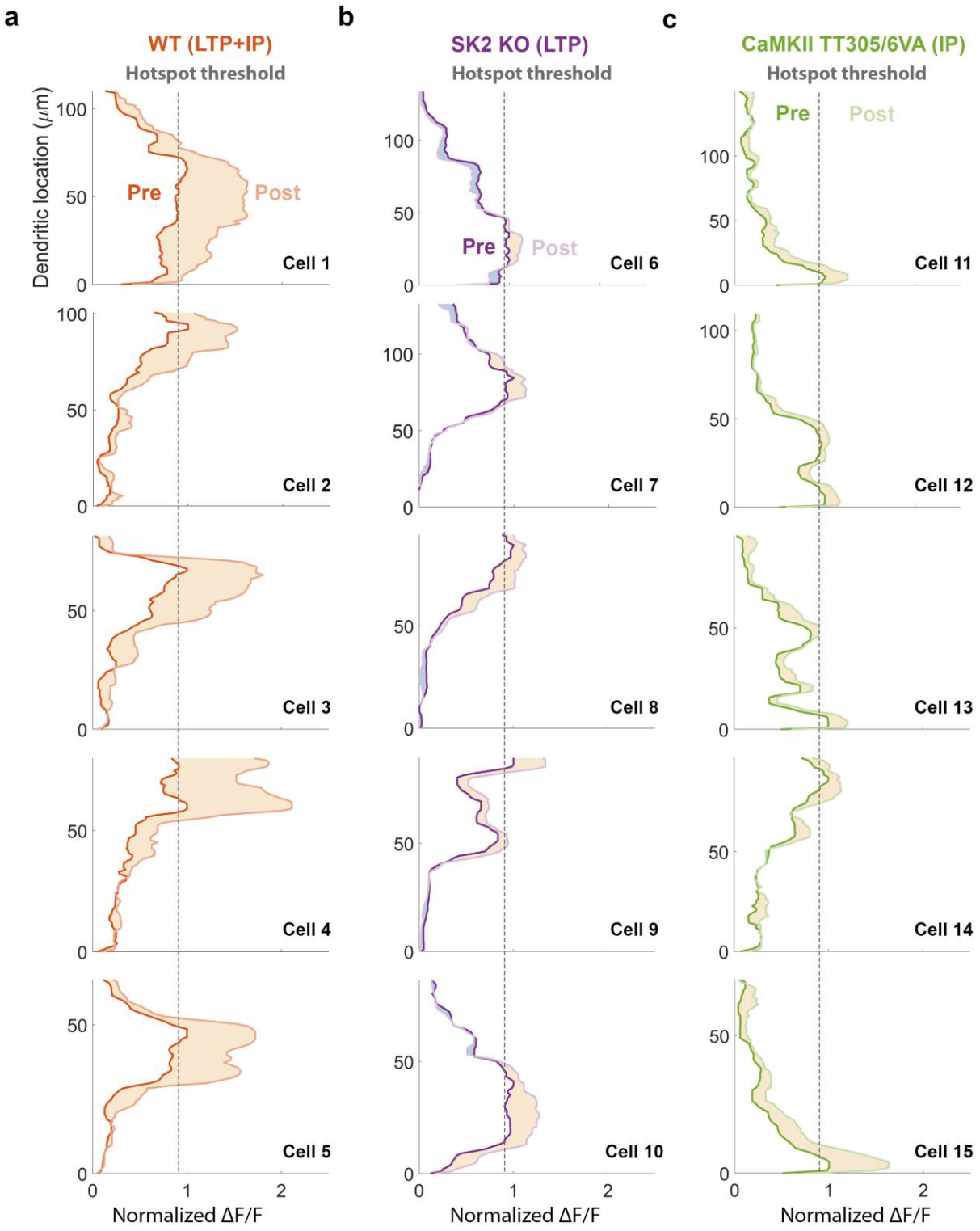

Supplementary Fig. 6 Representative spatial patterns of PF calcium response during pre-tetanus and early post-tetanus periods.

a-c. Representative linescan fluorescence signals of 5 individual PCs per genotype in addition to Fig. 6e-6g. The dark and light traces represent pre- and (early) post-tetanus data, respectively. The dashed lines indicate hotspot area (pixels with >0.9 normalized pre-tetanus ΔF/F).

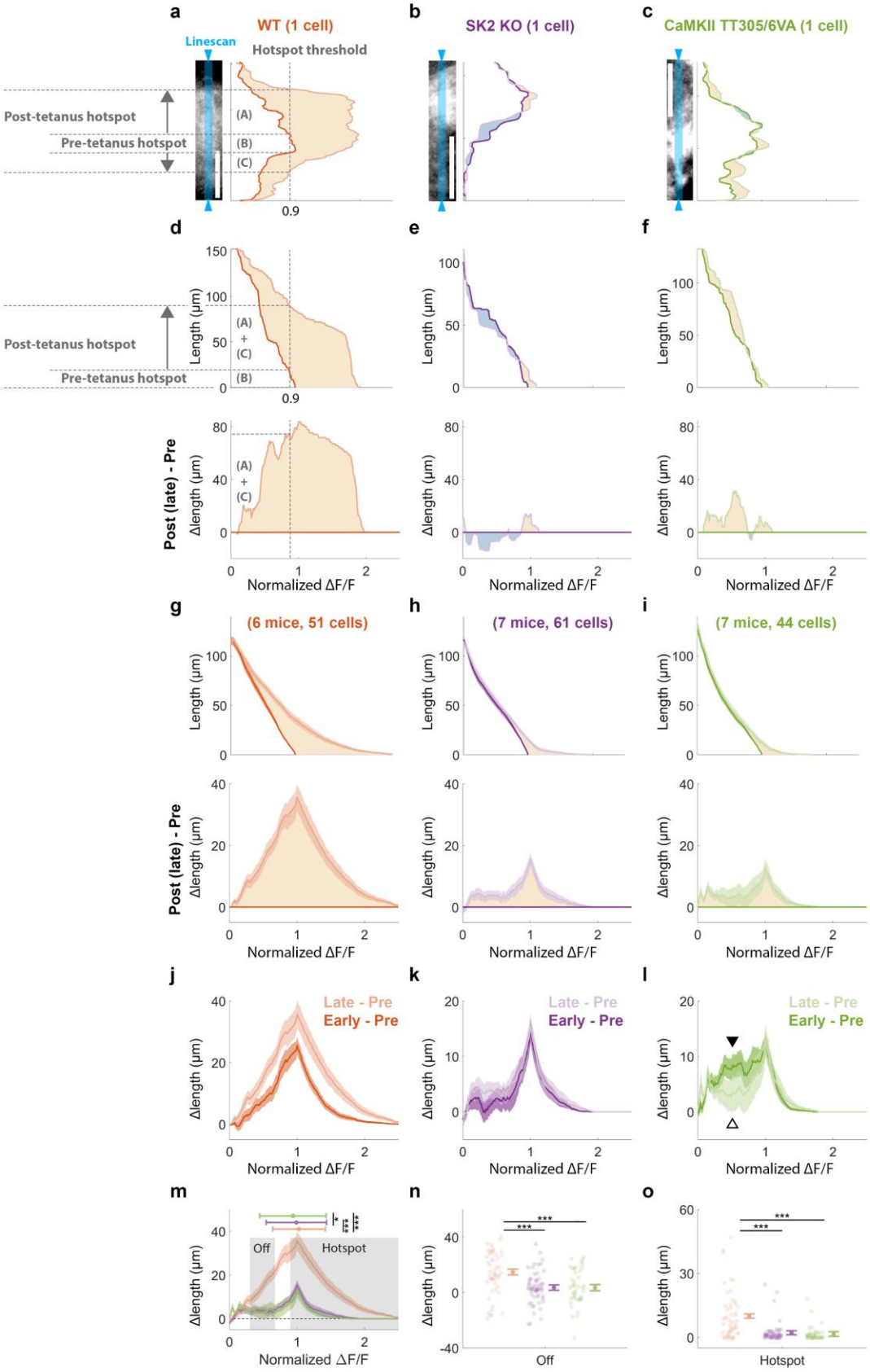
a
WT (1 cell)
Linescan
Hotspot threshold
Post-tetanus hotspot
Pre-tetanus hotspot
(A)
(B)
(C)
0.9
b
SK2 KO (1 cell)
c
CaMKII TT305/6VA (1 cell)
d
e
f
Length (µm)
Post-tetanus hotspot
Pre-tetanus hotspot
(A) + (C)
Post (late) - Pre
Δlength (µm)
Normalized ΔF/F
g
(6 mice, 51 cells)
h
(7 mice, 61 cells)
i
(7 mice, 44 cells)
j
Late - Pre
Early - Pre
k
l
m
Off
Hotspot
n
o
***

1146

Supplementary Fig. 7 Genotypic spatial patterns of PF calcium response during pre-tetanus and late post-tetanus periods.

a-c. Representative two-photon images of individual PCs from each genotype are shown in the left panels, with corresponding linescan fluorescence signals in the right panels. Blue shaded areas depict the linescan recording site. The dark and light traces represent pre- and (late) post-tetanus data collected from the same cells depicted in Fig. 6e-6g. The hotspot area (pixels with >0.9 normalized pre-tetanus ΔF/F) expanded from a length of (B) during the pre-tetanus period to a combined length of (A)+(B)+(C) during the post-tetanus period, thus the (A)+(C) represents Δlengths.

d-f. The top panel displays the cumulative lengths of dendrites as a function of fluorescence level, while the bottom panel displays the corresponding Δlengths of the representative data shown in **a-c**. Cumulative lengths were obtained by summing up the dendritic length exhibiting the given fluorescence level, depicted as the dashed lines in **a** and the top panel of **d**. Δlengths were calculated by subtracting post-tetanus from pre-tetanus cumulative length, as indicated by the dashed line in **d**.

g-i. For all cells from all mice in each group, mean ± SEM of cumulative lengths (top panel) and Δlengths (bottom panel) as in **d-f**.

j-l. Mean ± SEM of Δlengths between pre- and early post-tetanus periods, as well as between pre- and late post-tetanus periods, as depicted in Fig. 6k-6m and **g-i**, respectively. The triangles in l indicate a decrease in Δlength from early post-tetanus period (solid triangle) to late post-tetanus period (open triangle).

m. Superimposed genotype Δlengths obtained from the bottom panel of **g-i**. The horizontal bar represents the median ± median absolute deviation of the distribution. Asterisks denote significance in distribution shift using Dunn & Sidák's approach (*, $p < 0.05$; **, $p < 0.01$; ***, $p < 0.001$) following Kruskal-Wallis test ($H[2] = 57.12$, $p < 0.001$).

n-o. Mean ± SEM of Δlengths, calculated from the off-hotspot (**n**) and hotspot (**o**) as grey shaded areas shown in **j**, with individual cell values alongside. (One-way ANOVA: off-hotspot, $F[2,153] = 9.77$, $p < 0.001$; hotspot, $F[2,153] = 21.37$, $p < 0.001$) Asterisks denote the significance levels of post hoc comparisons using Tukey's HSD (*, $p < 0.05$; **, $p < 0.01$; ***, $p < 0.001$).

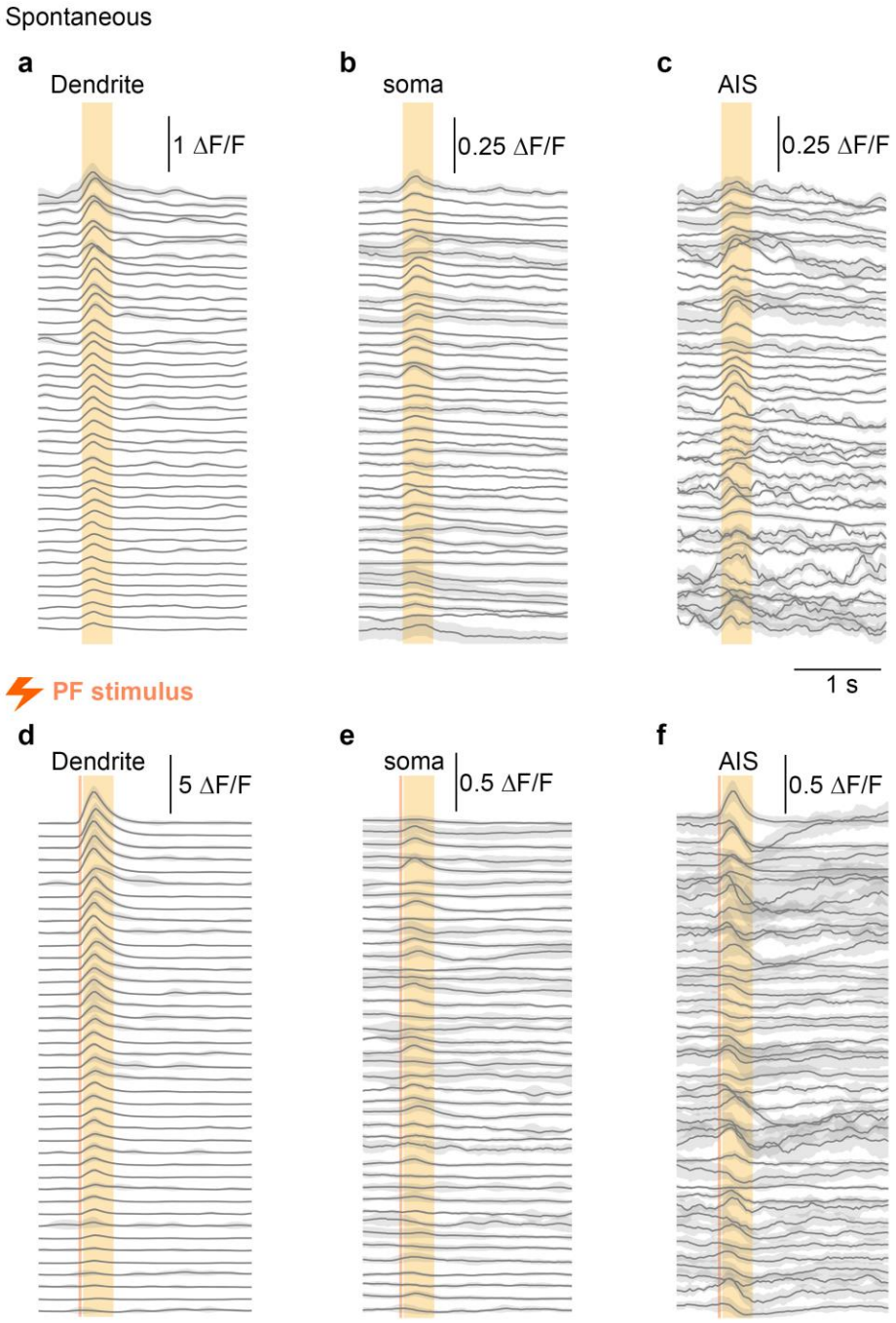

Supplementary Fig. 8 Average calcium transients in dendrite, soma and AIS for each PC. **a-c.** Average spontaneous calcium transients in dendrite (**a**), soma (**b**) and AIS (**c**) for each PC. Cells are sorted based on the amplitude of dendritic signals.
d-f. Average PF-evoked calcium transients in dendrite (**d**), soma (**e**) and AIS (**f**) for each PC. Cells are sorted based on the amplitude of dendritic signals.